Single electrons from heavy-flavor mesons in relativistic heavy-ion collisions

Taesoo Song,[1,2,3,*] Hamza Berrehrah,[1,2] Juan M. Torres-Rincon,[2] Laura Tolos,[2,4] Daniel Cabrera,[5] Wolfgang Cassing,[3] and Elena Bratkovskaya[1,6]

[1]*Institute for Theoretical Physics, Johann Wolfgang Goethe Universität, Frankfurt am Main, Germany*

[2]*Frankfurt Institute for Advanced Studies, Johann Wolfgang Goethe Universität, Frankfurt am Main, Germany*

[3]*Institut für Theoretische Physik, Universität Gießen, Gießen, Germany*

[4]*Institut de Ciencies de l'Espai (IEEC/CSIC), Campus Universitat Autonoma de Barcelona, Carrer de Can Magrans, s/n, E-08193 Bellaterra, Spain*

[5]*Instituto de Física Corpuscular (IFIC), Centro Mixto Universidad de Valencia - CSIC, Institutos de Investigación de Paterna, Apartado Correos 22085, E-46071 Valencia, Spain*

[6]*GSI Helmholtzzentrum für Schwerionenforschung GmbH, Darmstadt, Germany*

(Received 27 May 2016; revised manuscript received 27 April 2017; published 7 July 2017)

We study the single electron spectra from D- and B-meson semileptonic decays in Au + Au collisions at $\sqrt{s_{\rm NN}} = 200$, 62.4, and 19.2 GeV by employing the parton-hadron-string dynamics (PHSD) transport approach that has been shown to reasonably describe the charm dynamics at Relativistic Heavy Ion Collider and Large Hadron Collider energies on a microscopic level. In this approach the initial charm and bottom quarks are produced by using the PYTHIA event generator which is tuned to reproduce the fixed-order next-to-leading logarithm calculations for charm and bottom production. The produced charm and bottom quarks interact with off-shell (massive) partons in the quark-gluon plasma with scattering cross sections which are calculated in the dynamical quasiparticle model that is matched to reproduce the equation of state of the partonic system above the deconfinement temperature T_c. At energy densities close to the critical energy density ($\approx$0.5 GeV/fm^3) the charm and bottom quarks are hadronized into D and B mesons through either coalescence or fragmentation. After hadronization the D and B mesons interact with the light hadrons by employing the scattering cross sections from an effective Lagrangian. The final D and B mesons then produce single electrons through semileptonic decay. We find that the PHSD approach well describes the nuclear modification factor $R_{\rm AA}$ and elliptic flow v_2 of single electrons in d + Au and Au + Au collisions at $\sqrt{s_{\rm NN}} = 200$ GeV and the elliptic flow in Au + Au reactions at $\sqrt{s_{\rm NN}} = 62.4$ GeV from the PHENIX Collaboration, however, the large $R_{\rm AA}$ at $\sqrt{s_{\rm NN}} = 62.4$ GeV is not described at all. Furthermore, we make predictions for the $R_{\rm AA}$ of D mesons and of single electrons at the lower energy of $\sqrt{s_{\rm NN}} = 19.2$ GeV. Additionally, the medium modification of the azimuthal angle ϕ between a heavy quark and a heavy antiquark is studied. We find that the transverse flow enhances the azimuthal angular distributions close to $\phi = 0$ because the heavy flavors strongly interact with nuclear medium in relativistic heavy-ion collisions and almost flow with the bulk matter.

DOI: 10.1103/PhysRevC.96.014905

I. INTRODUCTION

Relativistic heavy-ion collisions are the experiments of choice to generate hot and dense matter in the laboratory. Whereas in low energy collisions one produces dense nuclear matter with moderate temperature at large baryon chemical potential μ_B, ultrarelativistic collisions at Relativistic Heavy Ion Collider (RHIC) or Large Hadron Collider (LHC) energies produce extremely hot matter at small baryon chemical potential. In order to explore the phase diagram of strongly interacting matter as a function of T and μ_B both types of collisions are mandatory. According to lattice calculations of quantum chromodynamics (lQCD) [1–3], the phase transition from hadronic to partonic degrees of freedom (at vanishing baryon chemical potential $\mu_B = 0$) is a crossover. This phase transition is expected to turn into a first order transition at a critical point (T_r, μ_r) in the phase diagram with increasing baryon chemical potential μ_B. Since this critical point cannot be determined theoretically in a reliable way the beam energy scan (BES) program performed at the RHIC by the STAR Collaboration aims to find the critical point and the phase boundary by gradually decreasing the collision energy [4,5].

Since the hot and dense matter produced in relativistic heavy-ion collisions appears only for a couple of fm/c, it is a big challenge for experiments to investigate its properties. The heavy-flavor mesons are considered to be promising probes in this search since the production of heavy flavor requires a large energy-momentum transfer. Thus it takes place early in the heavy-ion collisions, and—due to the large energy-momentum transfer—should be described by perturbative quantum chromodynamics (pQCD). The produced heavy flavor then interacts with the hot dense matter (of partonic or hadronic nature) by exchanging energy and momentum. As a result, the ratio of the measured number of heavy flavors in heavy-ion collisions to the expected number in the absence of nuclear or partonic matter, which is the definition of $R_{\rm AA}$ (cf. Sec. VII), is suppressed at high transverse momentum, and the elliptic flow of heavy flavor is generated by the interactions in noncentral heavy-ion collisions. Although it had been expected

*song@fias.uni-frankfurt.de

 ©2017 American Physical Society

that the R_{AA} of heavy flavor is less suppressed and its elliptic flow is smaller as compared to the corresponding quantities for light hadrons, the experimental data show that the suppression of heavy-flavor hadrons at high transverse momentum and its elliptic flow v_2 are comparable to those of light hadrons [6,7]. This is a puzzle for heavy-flavor production and dynamics in relativistic heavy-ion collisions as pointed out by many groups [8–22]. For recent reviews we refer the reader to Refs. [23,24].

Since the heavy-flavor interactions are closely related to the dynamics of the partonic or hadronic degrees of freedom due to their mutual interactions, a proper description of the relativistic heavy-ion collisions and their bulk dynamics is necessary. In this study we employ the parton-hadron-string dynamics (PHSD) approach, which differs from the conventional Boltzmann-type models in the aspect [25] that the degrees of freedom for the QGP phase are off-shell massive strongly interacting quasiparticles that generate their own mean-field potential. The masses of the dynamical quarks and gluons in the QGP are distributed according to spectral functions whose pole positions and widths, respectively, are defined by the real and imaginary parts of their self-energies [26]. The partonic propagators and self-energies, furthermore, are defined in the dynamical quasiparticle model (DQPM) in which the strong coupling and the self-energies are fitted to lattice QCD results.

We recall that the PHSD approach has successfully described numerous experimental data in relativistic heavy-ion collisions from the Super Proton Synchrotron (SPS) to LHC energies [25–28]. More recently, the charm production and propagation has been explicitly implemented in the PHSD and detailed studies on the charm dynamics and hadronization/fragmention have been performed at top RHIC and LHC energies in comparison to the available data [29,30]. In the PHSD approach the initial charm and anticharm quarks are produced by using the PYTHIA event generator [31] which is tuned to the transverse momentum and rapidity distributions of charm and anticharm quarks from the fixed-order next-to-leading logarithm (FONLL) calculations [32]. The produced charm and anticharm quarks interact in the QGP with off-shell partons and are hadronized into D mesons close to the critical energy density for the crossover transition either through fragmentation or coalescence. We stress that the coalescence is a genuine feature of heavy-ion collisions and does not show up in $p + p$ interactions. The hadronized D mesons then interact with light hadrons in the hadronic phase until freeze-out and subsequently undergoes semileptonic decay. We have found that the PHSD approach, which has been applied for charm production in Au + Au collisions at $\sqrt{s_{NN}} = 200$ GeV [29] and in Pb + Pb collisions at $\sqrt{s_{NN}} = 2.76$ TeV [30], describes the R_{AA} as well as the v_2 of D mesons in reasonable agreement with the experimental data from the STAR Collaboration [33,34] and from the ALICE Collaboration [35,36] when including the initial shadowing effect in the latter case.

In this work we, furthermore, extend the PHSD approach to bottom production in relativistic heavy-ion collisions. As in the case of charm, the initial bottom pair is produced by using the PYTHIA event generator, and the transverse momentum and rapidity distributions are adjusted to those from the FONLL calculations. Also the scattering cross sections of bottom quarks with off-shell partons are calculated in the DQPM on the same basis as the c quarks. The bottom quarks are hadronized into B mesons near the critical energy density in the same way as charm quarks. Furthermore, the scattering cross sections of B mesons with light hadrons (in the hadronic phase) are calculated from a similar effective Lagrangian as used for D mesons.

Presently, there are no exclusive experimental data for B-meson production from relativistic heavy-ion collisions. The PHENIX Collaboration instead measured the single electrons which are produced through the semileptonic decay of D and B mesons in Au + Au collisions at $\sqrt{s_{NN}} = 200$ and 62.4 GeV [37–39]. In this work we will study the bottom production through the single electrons in Au + Au collisions at $\sqrt{s_{NN}} = 200$ and 62.4 GeV by using the extended PHSD. Additionally, we make predictions for D-meson and single electron production at the much lower energy $\sqrt{s_{NN}} = 19.2$ GeV while we compare with the experimental results available at $\sqrt{s_{NN}} = 200$ and 62.4 GeV. Finally, we study the medium modification of the azimuthal angle ϕ of a heavy-flavor pair in relativistic heavy-ion collisions by the interactions with the partonic or hadronic medium.

This paper is organized as follows: The production of heavy mesons and their semileptonic decay in $p + p$ collisions is described in detail and compared with experimental data in Sec. II. The initial production of heavy quarks is explained in Sec. III including the shadowing effect in relativistic heavy-ion collisions. We then present the heavy quark interactions in the QGP, their hadronization, and hadronic interactions, respectively, in Secs. IV–VI. Finally, we show our results in Sec. VII in comparison with the experimental data while a summary closes this study in Sec. VIII.

II. SINGLE ELECTRONS FROM HEAVY FLAVOR IN $p + p$ COLLISIONS

As pointed out in the Introduction the charm and bottom quark pairs are produced through initial hard nucleon-nucleon scattering in relativistic heavy-ion collisions. We employ the PYTHIA event generator to produce the heavy-quark pairs and modify their transverse momentum and rapidity such that they are similar to those from the FONLL calculations [32]. In the case of $p + p$ collisions at the top RHIC energy of $\sqrt{s} = 200$ GeV, the transverse momentum and the rapidity of the charm quark from the PYTHIA event generator are reduced by 10% and 16% [29], respectively, and those of the bottom quark are unmodified. The transverse momentum of charm quarks at the invariant energy of $\sqrt{s} = 62.4$ GeV is modified to $p_T^* = p_T - 0.6\tanh(p_T/1.2\ \text{GeV})$, where p_T and p_T^*, respectively, are the original and modified transverse momenta, while the rapidity is reduced by 15% [32]. The transverse momentum and the rapidity of a bottom quark at the same energy are, respectively, reduced by 5% and enhanced by 15% [32]. The "MSEL" code in PYTHIA, which enables us to select a specific production channel, is taken to be the default value 1 for charm production, and 5 for bottom production.

Figures 1 and 2 show the p_T spectra and rapidity distributions of charm and bottom quarks in $p + p$ collisions at $\sqrt{s} =$ 200 and 62.4 GeV, where the dashed and solid lines are from

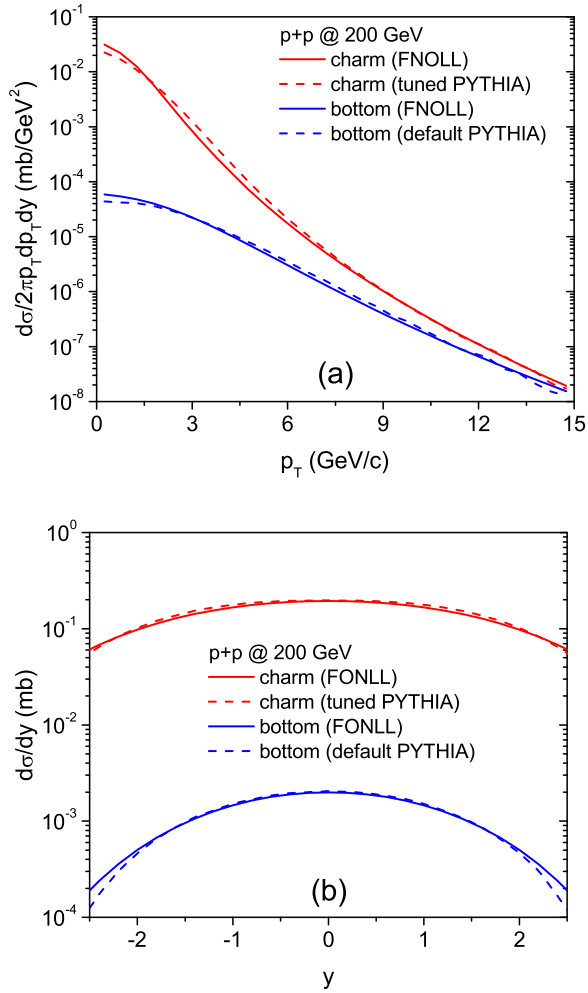

FIG. 1. The p_T spectra (a) and rapidity distributions (b) of charm and bottom quarks in $p + p$ collisions at $\sqrt{s} = 200$ GeV as generated by the tuned PYTHIA event generator (dashed) in comparison to those from FONLL (solid).

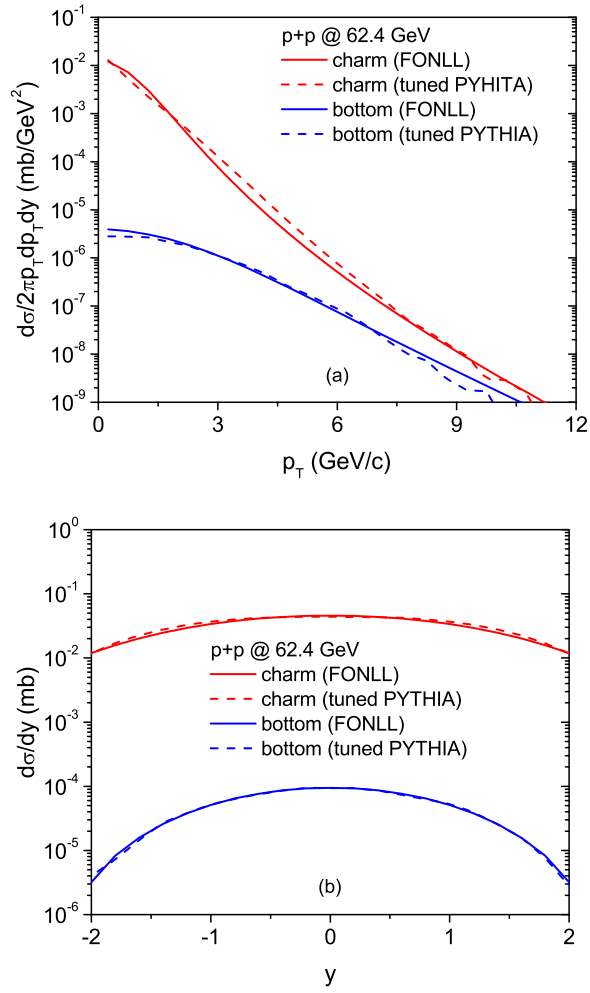

FIG. 2. The p_T spectra (a) and rapidity distributions (b) of charm and bottom quarks in $p + p$ collisions at $\sqrt{s} = 62.4$ GeV as generated by the tuned PYTHIA event generator (dashed) in comparison to those from FONLL (solid).

the tuned PYTHIA and FONLL calculations, respectively. The FONLL calculations are rescaled such that the total cross sections for charm production are 0.8 and 0.12 mb at $\sqrt{s} = 200$ and 62.4 GeV, respectively, from the measurement of the STAR Collaboration [40] and the interpolation of the PHSD [29]. The ratios of the bottom cross section to the charm cross section are taken to be 0.75% and 0.145% at the same energies as in the FONLL calculations [32]. We find that our tuned PYTHIA generator gives very similar charm and bottom distributions to those from FONLL calculations, which fixes the input from pQCD.

Furthermore, the produced charm and bottom quarks in hard nucleon-nucleon collisions are hadronized by emitting soft gluons, which is denoted by "fragmentation." We use the fragmentation function of Peterson which reads as [41]

$$D_Q^H(z) \sim \frac{1}{z[1 - 1/z - \epsilon_Q/(1-z)]^2}, \tag{1}$$

where z is the momentum fraction of the hadron H fragmented from the heavy quark Q while ϵ_Q is a fitting parameter which is taken to be $\epsilon_Q = 0.01$ for charm [29] and 0.004 for bottom [42]. Figure 3 shows the fragmentation functions of charm and bottom quarks as a function of the hadron momentum fraction z. Since the charm quark is much heavier than the soft emitted gluons, it takes a large momentum fraction in the fragmentation into a D meson. It is even more pronounced in the case of a bottom quark.

The chemical fractions of the charm quark decay into D^+, D^0, D^{*+}, D^{*0}, D_s, and Λ_c are taken to be 14.9, 15.3, 23.8, 24.3, 10.1, and 8.7% [30,43–45], respectively, and those of the bottom quark decay into B^-, $\bar{B}^0$, $\bar{B}^0{}_s$, and Λ_b are 39.9, 39.9, 11, and 9.2% [42]. After the momentum and the species of the fragmented particle are decided by Monte Carlo, the energy of the fragmented particle is adjusted to be on shell. Furthermore, the D^* mesons first decay into $D + \pi$ or $D + \gamma$, and then the D and B mesons produce single electrons through the semileptonic decay [46]. For simplicity, it is assumed that the transition amplitude for the semileptonic decay is constant and does not depend on particle momentum. Denoting the energy, momentum, and mass of a particle i by E_i, p_i, and m_i

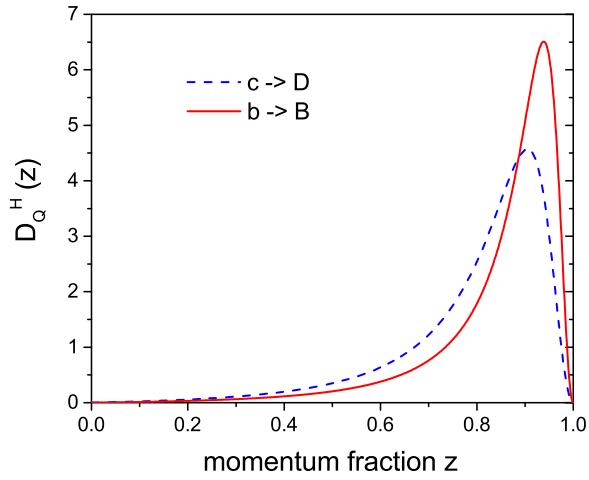

FIG. 3. Fragmentation functions of charm (dashed) and bottom (solid) as a function of the hadron momentum fraction z.

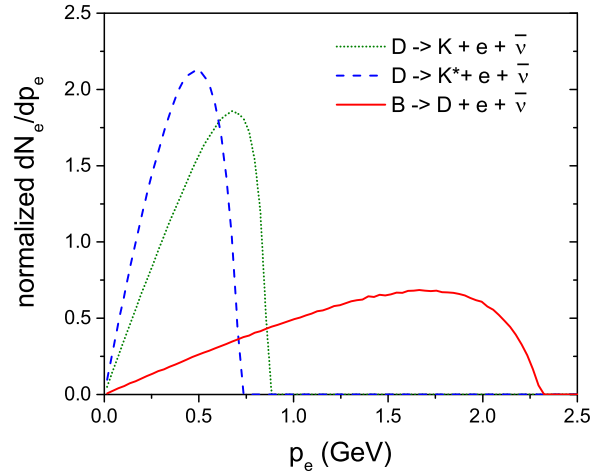

FIG. 4. The momentum distribution of single electrons from the decays $D \to K + e + \bar{\nu}_e$ (dotted), $D \to K^* + e + \bar{\nu}_e$ (dashed), and $B \to D + e + \bar{\nu}_e$ (solid) in the rest frame of the heavy meson.

in the decay $D \to K + e + \bar{\nu}_e$, the phase space for the final states $(K + e + \bar{\nu}_e)$ is then proportional to

$$\frac{d^3p_K}{E_K}\frac{d^3p_e}{E_e}\frac{d^3p_{\bar{\nu}}}{E_{\bar{\nu}}}\delta^4(p_D - p_K - p_e - p_{\bar{\nu}}). \tag{2}$$

In the center-of-mass frame of the leptons e and $\bar{\nu}_e$, it is simplified to

$$\sim \frac{d^3p_K}{E_K}dp_e\delta(E_D - E_K - 2p_e)$$
$$\sim \frac{d^3p_K}{E_K} + \text{energy conservation}, \tag{3}$$

because $E_e = E_{\bar{\nu}} = p_e$, assuming the leptons e and $\bar{\nu}_e$ to be massless. Finally, we perform a Lorentz boost to the rest frame of the D meson, where the solid angle of $\mathbf{p}_K$ is assumed to be isotropic:

$$\sim \frac{p_K^2}{E_K}dp_K + \text{energy conservation}. \tag{4}$$

The momentum p_K itself is decided by a random number as follows:

$$\text{random number} = \frac{\int_0^{p_K} dp\left(p^2/\sqrt{m_K^2 + p^2}\right)}{\int_0^{p_{\max}} dp\left(p^2/\sqrt{m_K^2 + p^2}\right)}, \tag{5}$$

where $p_{\max} = (m_D^2 - m_K^2)/(2m_D)$ is fixed by energy conservation. Accordingly, once p_K is fixed, the invariant mass of the lepton pair (e and $\bar{\nu}_e$), and then p_e in the center-of-mass frame of e and $\bar{\nu}_e$ are fixed. The solid angle of each particle is determined by Monte Carlo and its energy-momentum boosted back to the $p + p$ collision frame.

Figure 4 shows the momentum distribution of single electrons from the semileptonic decay of heavy mesons in the rest frame of the heavy meson. It shows that the single electron from the decay $B \to D + e + \bar{\nu}_e$ has the largest momentum and that from $D \to K^* + e + \bar{\nu}_e$ the lowest momentum according to the mass difference between the mother meson and the daughter meson. We also take into account the decay $D_s \to \phi + e + \bar{\nu}_e$, $D_s \to \eta + e + \bar{\nu}_e$, and $B_s \to D_s + e + \bar{\nu}_e$ [46]. The branching ratio of each decay channel is obtained from the Particle Data Group (PDG) [46]. This completes the description of the semileptonic decays.

In Fig. 5 we show the p_T spectrum of single electrons in $p + p$ collisions at $\sqrt{s} = 200$ GeV (a) and $\sqrt{s} = 62.4$ GeV (b). The figure shows that our results reproduce the experimental data at $\sqrt{s} = 200$ GeV from the PHENIX Collaboration [47] as well as at $\sqrt{s} = 62.4$ GeV from the Intersecting Storage Rings (ISR) [48]. We note, furthermore, that the contribution from B-meson decay is compatible to that from D-meson decay around $p_T \approx 4.5$ GeV at $\sqrt{s} = 200$ GeV, and around $p_T \approx 5.5$ GeV at $\sqrt{s} = 62.4$ GeV, respectively.

III. COLD NUCLEAR MATTER EFFECTS

The scattering cross section for heavy-quark pair production in a nucleon-nucleon collision is calculated by convoluting the partonic cross section with the parton distribution functions of the nucleon:

$$\sigma_{Q\bar{Q}}^{NN}(s) = \sum_{i,j}\int dx_1 dx_2 f_i^N(x_1,q) f_j^N(x_2,q)\sigma_{Q\bar{Q}}^{ij}(x_1x_2s,q), \tag{6}$$

where $f_i^N(x,q)$ is the distribution function of the parton i with the energy-momentum fraction x in the nucleon at scale q. The momentum fractions x_1 and x_2 are calculated from the transverse mass (M_T) and the rapidity (y) of the final-state particles by

$$x_1 = \frac{M_T}{E_{\text{cm}}}e^y, \quad x_2 = \frac{M_T}{E_{\text{cm}}}e^{-y}, \tag{7}$$

where E_{cm} is the nucleon-nucleon collision energy in the center-of-mass frame.

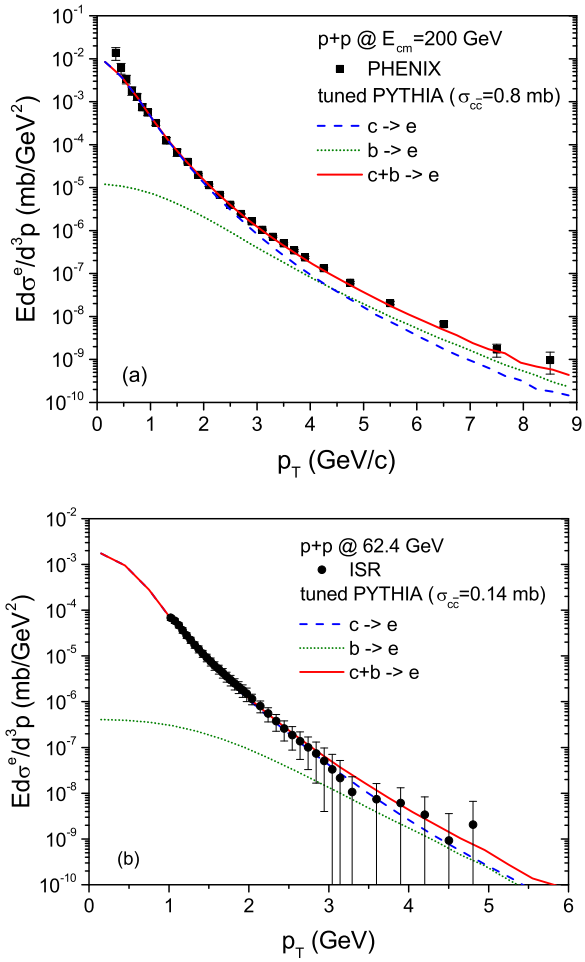

FIG. 5. The p_T spectrum of single electrons from charm and bottom mesons in $p+p$ collisions at $\sqrt{s}=200$ GeV (a) and $\sqrt{s}=62.4$ GeV (b) in comparison to the experimental data from Refs. [47,48].

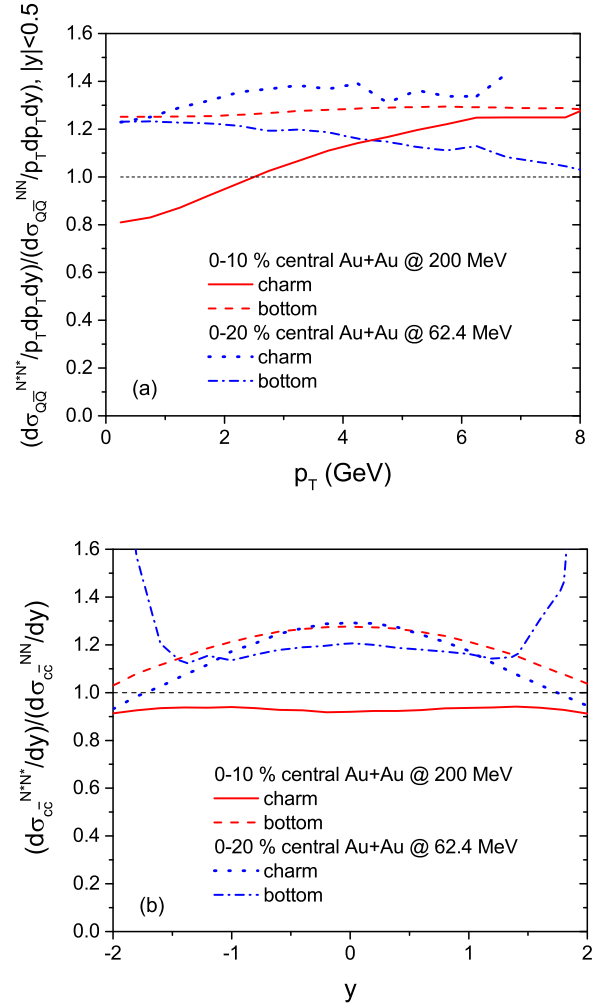

FIG. 6. The (anti)shadowing effect from EPS09 on charm and bottom production in 0–10% central Au + Au collisions at $\sqrt{s}=200$ GeV and in 0–20% central Au + Au collisions at $\sqrt{s}=62.4$ GeV as a function of p_T (a) and of y (b).

As it is well known the parton distribution function (PDF) is modified in a nucleus to

$$f_i^{N^*}(x,q) = R_i^A(x,q) f_i^N(x,q), \tag{8}$$

where N^* indicates a nucleon in nucleus A, and $R_i^A(x,q)$ is the ratio of the PDF of N^* to that of a free nucleon. The ratio $R_i^A(x,q)$ for a heavy nucleus A is lower than 1 at small momentum fraction x, and becomes larger than 1 with increasing x. The former phenomenon is called "shadowing" and the latter "antishadowing." When increasing x further, the ratio reaches a maximum and then decreases again, which is called the European Muon Collaboration (EMC) effect [49]. Finally, the ratio increases again close to $x=1$ due to Fermi motion. The EPS09 package [50] parametrizes this behavior of $R_i^A(x,q)$ and fits the heights and positions of the local extrema of the ratio to the experimental data from deep inelastic $l+A$ scattering, Drell-Yan dilepton production in $p+A$ collisions, and inclusive pion production in $d+$ Au and $p+p$ collisions at RHIC. We also employ the EPS09 package [50] in our PHSD calculations [30].

Furthermore, the (anti)shadowing effect is supposed to depend on the impact parameter in heavy-ion collisions such that it is strong in central collisions and weak in peripheral collisions. Therefore, we modify the ratio to [30]

$$R_i^A(r_\perp,x,q) = \frac{4}{3}\sqrt{1-\frac{r_\perp^2}{R_A^2}}\,R_i^A(x,q), \tag{9}$$

where R_A and $r_\perp$ are, respectively, the radius of the nucleus A and the transverse distance of the heavy-quark pair production from the nucleus center, while $R_i^A(x,q)$ is given by EPS09.

Substituting f_i^N in Eq. (6) by Eq. (8), the cross section for heavy quark production is modified to

$$\sigma_{Q\bar{Q}}^{N^*N^*}(s) = \sum_{i,j}\int dx_1 dx_2 R_i^A(x_1,q) R_j^A(x_2,q) \times f_i^N(x_1,q) f_j^N(x_2,q) \sigma_{Q\bar{Q}}^{ij}(x_1 x_2 s,q). \tag{10}$$

Figure 6 shows the ratio of the cross sections with (anti)shadowing to without (anti)shadowing. The scale q is

taken to be the average of the transverse mass of the heavy quark and that of the heavy antiquark. The total cross sections for charm and bottom production, respectively, decreases by 8% and increases by 21% in 0–10% central Au + Au collisions at $\sqrt{s} = 200$ GeV, and increases by 18% and 21% in 0–20% central Au + Au collisions at $\sqrt{s} = 64.2$ GeV. The ratio of the charm cross sections increases with increasing transverse momentum in 0–10% central Au + Au collisions at $\sqrt{s} = 200$ GeV, because $R_i^A(x,q)$ increases with increasing x in the (anti)shadowing region. In the case of bottom production, the corresponding x is larger and located close to the maximum of the antishadowing region. Therefore, the dependence of the (anti)shadowing effect on p_T or on x is monotonous. Since the momentum fraction x corresponding to bottom production at $\sqrt{s} = 200$ GeV is similar to that corresponding to charm production at $\sqrt{s} = 62.4$ GeV, the (anti)shadowing effect on both are similar in p_T as well as in rapidity y. Finally, the ratio of bottom production at $\sqrt{s} = 62.4$ GeV decreases with increasing p_T, because the corresponding momentum fraction x moves towards the EMC effect region, where $R_i^A(x,q)$ decreases with increasing x.

Additionally, we study the Cronin effect on the production of initial heavy quarks in relativistic heavy-ion collisions. A heavy-flavor pair is produced by a hard scattering of partons, mainly, gluons. On the other hand, the gluons may interact with other nucleons before participating in heavy-flavor production. This scattering enhances the transverse momentum of gluons and consequently also the transverse momentum of the heavy-quark pair. As a result, the distribution in transverse momentum of heavy flavor is smeared in the collisions of nuclei A and B as [16,51]

$$f_{AB}^{Q\bar{Q}}(\vec{p}_T) = \frac{1}{\pi\langle p_T'^2\rangle}\int d^2p_T' \exp\left[\frac{-p_T'^2}{\langle p_T'^2\rangle}\right] f_{NN}^{Q\bar{Q}}(\vec{p}_T - \vec{p}_T') \tag{11}$$

with the broadening width in transverse momentum [52]

$$\langle p_T'^2\rangle = \frac{0.225\ln^2(\mu/\mathrm{GeV})}{1+\ln(\mu/\mathrm{GeV})}\left(N_A^{\mathrm{coll}} + N_B^{\mathrm{coll}}\right)(\mathrm{GeV}^2), \tag{12}$$

where the scale μ is taken to be twice the heavy-quark mass and N_A^{coll} and N_B^{coll} are the numbers of nucleon-nucleon binary collisions of two nucleons in nucleus A and B before they produce a heavy-quark pair.

We assume that the transverse momentum change $\vec{p}_T'$ is shared equally by the heavy quark and the heavy antiquark (from the same pair). This is different by a factor $1/\sqrt{2}$ from other studies where the heavy quark and heavy antiquark are completely independent of each other, even though they stem from the same pair [16,53]. This difference reduces the importance of the Cronin effect on open heavy flavor in heavy-ion collisions.

Figure 7 shows the modifications of the charm transverse momentum due to the shadowing and Cronin effects in heavy-ion collisions at $\sqrt{s} = 200$ GeV. Since the path length of nucleons, which participate heavy-flavor production, is twice as large in Au + Au collisions as compared to d + Au collisions and both shadowing and Cronin effects are proportional to the path length, the cold nuclear matter effects are roughly twice

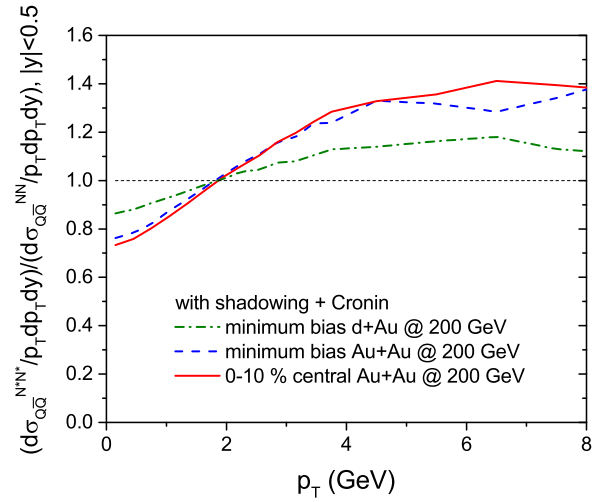

FIG. 7. The modifications of the charm transverse momentum due to the shadowing and Cronin effects in minimum bias d + Au and Au + Au collisions and 0–10% central Au + Au collisions at $\sqrt{s} = 200$ GeV.

in minimum bias Au + Au collisions compared to those in minimum bias d + Au collisions, as shown in Fig. 7. We can also see that the cold nuclear matter effects are stronger in central Au + Au collisions than in minimum bias reactions. Comparing with Fig. 6(a), we note that the Cronin effect enhances charm distribution additionally by about 10% at intermediate transverse momentum.

The light $p + A$ or $d + A$ collisions are well suited to investigate the cold nuclear matter effects, because thermal effects in such collisions will be of minor importance. We compare our cold nuclear matter effects with the experimental data for $d + Au$ collisions from the PHENIX Collaboration [54,55].

Figure 8(a) shows the R_{dAu} of single electrons at midrapidity ($|y| < 0.35$) and Fig. 8(b) that of single muons at forward ($1.4 < y < 2$, d direction) and backward ($-2 < y < -1.4$, Au direction). The kinematics for a single muon decay from D or B mesons is exactly the same as that for a single electron except that the maximum momentum of the daughter meson is substituted by

$$p_{\max} = \frac{\sqrt{\left\{m_D^2 - (m_K + m_\mu)^2\right\}\left\{m_D^2 - (m_K - m_\mu)^2\right\}}}{2m_D}$$

or

$$p_{\max} = \frac{\sqrt{\left\{m_B^2 - (m_D + m_\mu)^2\right\}\left\{m_B^2 - (m_D - m_\mu)^2\right\}}}{2m_B},$$

respectively.

Figure 8 shows that the interactions of heavy flavor with cold nuclear matter generate a maximum in R_{dAu} around $p_{\mathrm{T}} = 1.5$ GeV. More interaction and larger coalescence probability of heavy flavor in the Au direction split the R_{dAu} in forward and backward rapidities, but the separation is not enough to explain the experimental data. The shadowing effects help the separation, because the heavy flavors at forward rapidities are

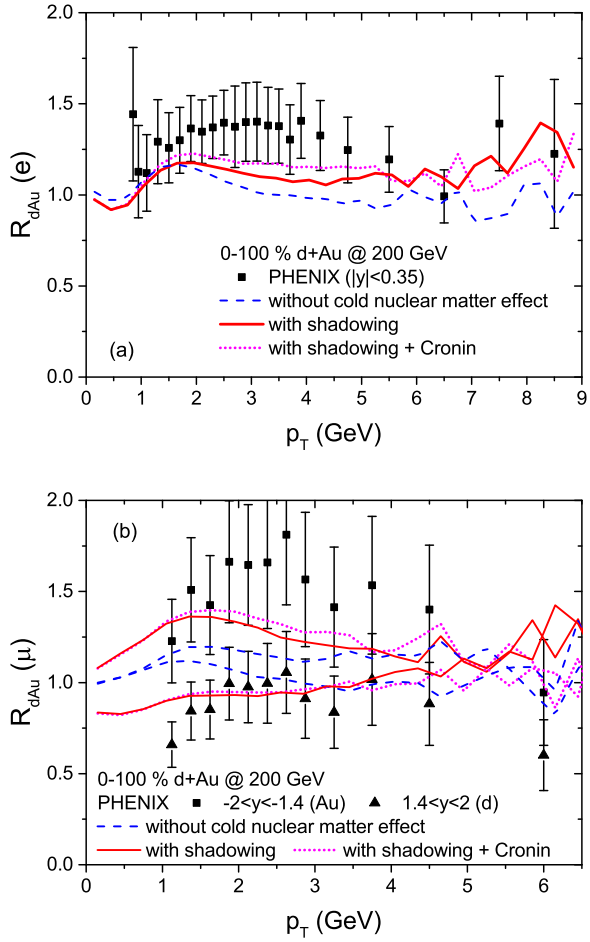

FIG. 8. R_{dAu} of single electrons at midrapidity and that of single muons at forward/backward rapidities in minimum-bias d + Au collisions at $\sqrt{s_{\mathrm{NN}}} = 200$ GeV. Dashed, solid, and dotted lines correspond to the R_{dAu} without cold nuclear matter effect, with the shadowing effect, and with both shadowing and Cronin effects, respectively. Experimental data are given by the PHENIX Collaboration [54,55].

contributed by gluons with small x in the Au nucleus and those in backward rapidities by gluons with large x. Since $R_i^A(x,q)$ in Eq. (8) increases with larger x, the production of heavy flavor is suppressed at forward rapidity and enhanced at backward rapidity. Figure 8 also shows that the Cronin effect helps our results to come closer to the experimental data at midrapidity as well as at forward/backward rapidities.

IV. HEAVY-QUARK INTERACTIONS IN THE QGP

In PHSD the baryon-baryon and baryon-meson collisions at high-energy produce strings. If the local energy density is above the critical energy density ($\sim$0.5 GeV/fm^3), the strings melt into quarks and antiquarks with masses determined by the temperature-dependent spectral functions from the DQPM [56]. Massive gluons are formed through flavor-neutral quark and antiquark fusion in line with the DQPM. In contrast to normal elastic scattering, off-shell partons may change their mass after the elastic scattering according to the local temperature T in the cell (or local space-time volume) where the scattering happens. This automatically updates the parton masses as the hot and dense matter expands, i.e., the local temperature decreases with time. The same holds true for the reaction chain from gluon decay to quark + antiquark ($g \rightarrow q + \bar{q}$) and the inverse reaction ($q + \bar{q} \rightarrow g$) following detailed balance.

Due to the finite spectral width of the partonic degrees of freedom, the parton spectral function has timelike as well as spacelike parts. The timelike partons propagate in space-time within the light cone while the spacelike components are attributed to a scalar potential energy density [25]. The gradient of the potential energy density with respect to the scalar density generates a repulsive force in relativistic heavy-ion collisions and plays an essential role in reproducing experimental flow data and transverse momentum spectra (see Ref. [26] for a review).

However, the spectral function of a heavy quark or heavy antiquark cannot be fitted from lattice QCD data on thermodynamical properties because the contribution from a heavy quark or heavy antiquark to the lattice entropy is small. Our recent study shows that the scattering cross sections of heavy quark moderately depend on the spectral function of heavy quark, and the repulsive force for charm quarks—as originating from the scalar potential energy density—is disfavored by experimental data [30]. This is expected since the width of the spectral function for a charm quark is very small compared to the pole mass such that spacelike contributions to the (potential) energy density are practically vanishing. Therefore, we assume in this study that the heavy quark has a constant (on-shell) mass: the charm quark mass is taken to be 1.5 GeV and the bottom quark mass as 4.8 GeV, but the light quarks/antiquarks as well as gluons are treated fully off shell.

The heavy quarks and antiquarks produced in early hard collisions—as described above—interact with the dressed lighter off-shell partons in the QGP. The cross sections for the heavy-quark scattering with massive off-shell partons have been calculated by considering explicitly the mass spectra of the final state particles in Refs. [57,58]. The elastic scattering of heavy quarks in the QGP is treated by including the nonperturbative effects of the strongly interacting quark-gluon plasma (sQGP) constituents, i.e., the temperature-dependent coupling $g(T/T_c)$ which rises close to T_c, the multiple scattering, etc. The multiple strong interactions of quarks and gluons in the sQGP are encoded in their effective propagators with broad spectral functions (imaginary parts). As pointed out above, the effective propagators, which can be interpreted as resummed propagators in a hot and dense QCD environment, have been extracted from lattice data in the scope of the DQPM [56]. We recall that the divergence encountered in the t-channel scattering is cured self-consistently, since the infrared regulator is given by the finite DQPM gluon mass and width. For further details we refer the reader to Refs. [57,58].

Figure 9 compares the total (a) and differential (b) scattering cross sections of charm and bottom quarks with a light quark at $T = 1.5T_c$. It shows that the total cross section of a charm quark is similar to that of the bottom quark apart from different threshold energies. However, the differential scattering cross section of a bottom quark is more peaked in

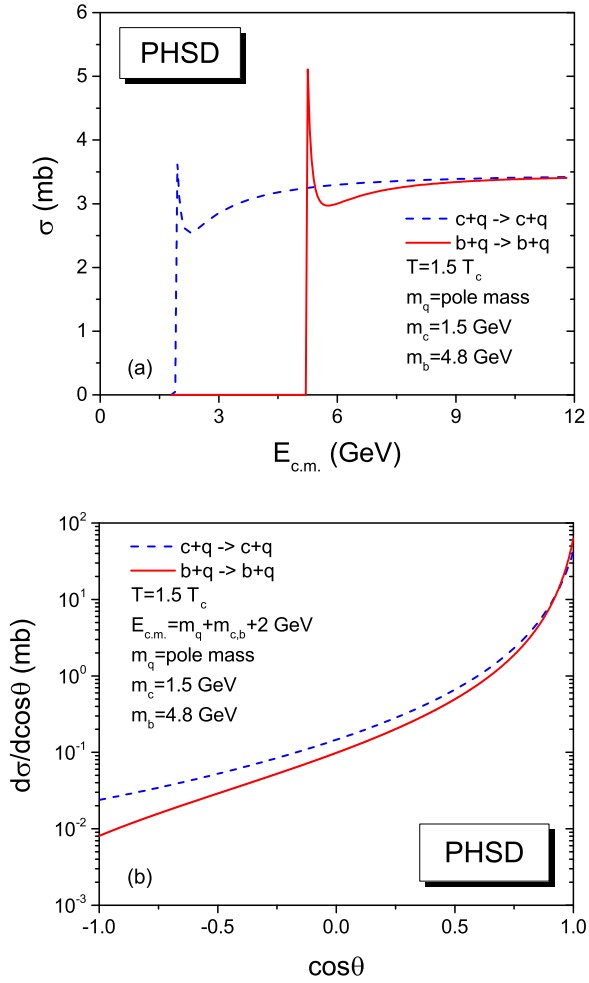

FIG. 9. The total (a) and differential (b) scattering cross sections for the reactions $c + q \to c + q$ and $b + q \to b + q$ employed in the PHSD have been multiplied by a factor of 2 [57,58].

the forward direction, compared to that of a charm quark. This is expected because it is harder to change the direction of motion of a bottom quark in elastic scattering due to the larger mass.

We note that the scattering cross sections of heavy quark used in the PHSD calculations are twice larger than from the Born diagrams of the DQPM in order to achieve consistency with the lQCD data from Refs. [30,59], however, they differ substantially from the pQCD scenario [60].

V. HEAVY-QUARK HADRONIZATION

The heavy-quark hadronization in heavy-ion collisions is realized via "dynamical coalescence" and fragmentation. Here dynamical coalescence means that the probability to find a coalescence partner is defined by Monte Carlo in the vicinity of the critical energy density $0.4 \leqslant \epsilon \leqslant 0.75$ GeV/fm^3 as explained below. We note that such a dynamical realization of heavy-quark coalescence is in line with the dynamical hadronization of light quarks in the PHSD and differs from the "spontaneous" coalescence used in our early work [29] when heavy quarks are forced to hadronize at a critical energy density $\epsilon_c = 0.5$ GeV/fm^3 via coalescence or fragmentation by Monte Carlo. Indeed, the dynamical realization gives some window in energy density to find the proper light partner and leads to an enhancement of the heavy-quark fraction that hadronizes via coalescence.

In PHSD all antiquarks neighboring in phase space are candidates for the coalescence partner of a heavy quark. From the distances in coordinate and momentum spaces between the heavy quark and light antiquark (or vice versa), the coalescence probability is given by [61]

$$f(\boldsymbol{\rho},\mathbf{k}_\rho) = \frac{8g_H}{6^2}\exp\left[-\frac{\boldsymbol{\rho}^2}{\delta^2} - \mathbf{k}_\rho^2\delta^2\right], \tag{13}$$

where g_H is the degeneracy of the heavy meson, and

$$\boldsymbol{\rho} = \frac{1}{\sqrt{2}}(\mathbf{r}_1 - \mathbf{r}_2), \quad \mathbf{k}_\rho = \sqrt{2}\frac{m_2\mathbf{k}_1 - m_1\mathbf{k}_2}{m_1 + m_2}, \tag{14}$$

with m_i, $\mathbf{r}_i$, and $\mathbf{k}_i$ denoting the mass, position, and momentum of the quark or antiquark i in the center-of-mass frame, respectively. The width parameter δ is related to the root-mean-square radius of the produced heavy meson through

$$\langle r^2\rangle = \frac{3}{2}\frac{m_1^2 + m_2^2}{(m_1 + m_2)^2}\delta^2, \tag{15}$$

where m_1 and m_2 are respectively the masses of quark and antiquark. Since this prescription gives a larger coalescence probability at low transverse momentum, the radius is taken to be 0.9 fm for a charm quark as well as for a bottom quark [29]. We also include the coalescence of charm quarks into highly excited states, $D_0^*(2400)^0$, $D_1(2420)^0$, and $D_2^*(2460)^{0,\pm}$ and the coalescence of bottom quarks into $B_1(5721)^{+,0}$, $B_2^*(5747)^{+,0}$, and $B(5970)^{+,0}$, which are respectively assumed to immediately decay to D (or D^*) and π and to B (or B^*) and π after hadronization as described in Ref. [29].

Summing up the coalescence probabilities from all candidates, whether or not the heavy quark or heavy antiquark hadronizes by coalescence, and which quark or antiquark among the candidates will be the coalescence partner, is decided by Monte Carlo. If a random number is above the sum of the coalescence probabilities, it is tried again in the next time step until the local energy density is lower than 0.4 GeV/fm^3. The heavy quark or heavy antiquark, which does not succeed to hadronize by coalescence, then hadronizes through fragmentation as in $p + p$ collisions.

Figure 10 shows the coalescence probabilities of charm and bottom quarks at midrapidity ($|y| < 0.5$) as functions of transverse momentum (a) and of transverse velocity (b) in 0–10% central Au + Au collisions at $\sqrt{s_{\rm NN}} = 200$ GeV. Since a heavy quark with a large transverse momentum has a smaller chance to find a coalescence partner close by in phase space, the coalescence probability decreases with increasing transverse momentum. It appears from the upper figure (a) that the coalescence probability of a bottom quark is larger than that of a charm quark. It emerges, however, because the bottom quark is much heavier than the charm quark. The lower figure (b) clearly shows that the coalescence probability is similar for

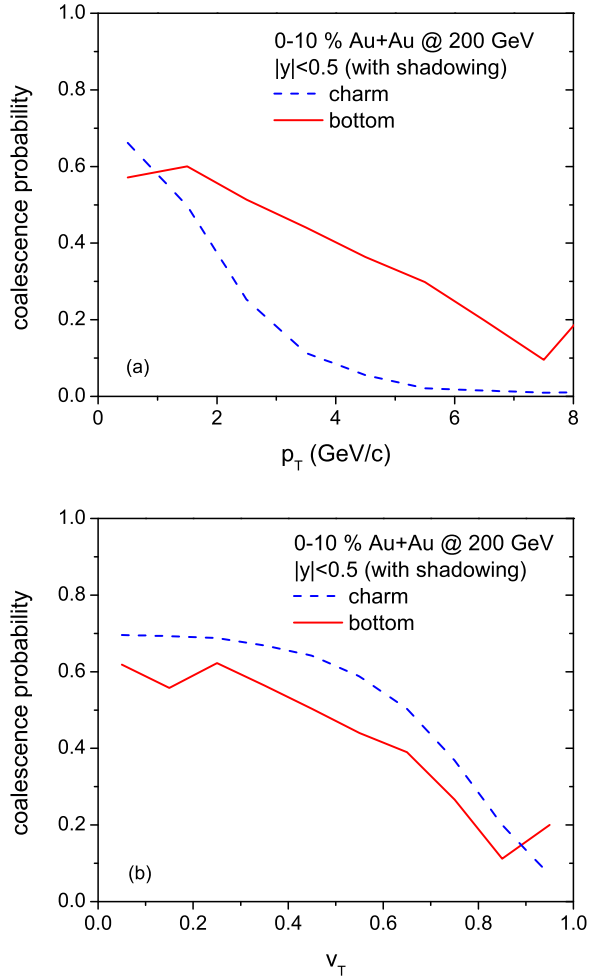

FIG. 10. Coalescence probability of charm and bottom quarks at midrapidity ($|y| < 0.5$) as functions of transverse momentum (a) and of transverse velocity (b) in 0–10% central Au + Au collisions at $\sqrt{s_{\rm NN}} = 200$ GeV taking into account the shadowing effect.

a bottom or charm quark, when it is expressed as a function of the transverse velocity v_T.

VI. INTERACTIONS OF CHARM AND BOTTOM MESONS WITH THE HADRONIC MEDIUM

After the hadronization of heavy quarks and their subsequent decay into D, D^*, B, and B^* mesons, the final stage of the evolution concerns the interaction of these states with the hadrons conforming the expanding bulk medium. A realistic description of the hadron-hadron scattering—potentially affected by resonant interactions—includes collisions with the states $\pi, K, \bar{K}, \eta, N, \bar{N}, \Delta, \bar{\Delta}$. A description of their interactions has been developed in Refs. [62–70] using effective field theory. Moreover, after the application of an effective theory, one should implement to the scattering amplitudes a unitarization method to better control the behavior of the cross sections at moderates energies.

The details of the interaction for the four heavy states follow quite in parallel by virtue of the "heavy-quark spin-flavor symmetry." It accounts for the fact that if the heavy masses are much larger than any other typical scale in the system, like Λ_{QCD}, temperature, and the light hadron masses, then the physics of the heavy subsystem is decoupled from the light sector, and the former is not dependent on the mass nor on the spin of the heavy particle. This symmetry is exact in the ideal limit $m_Q \to \infty$, with m_Q being the mass of the heavy quark confined in the heavy hadron. In the opposite limit $m_Q \to 0$, one can exploit the chiral symmetry of the QCD Lagrangian to develop an effective realization for the light particles. This applies to the pseudoscalar meson octet $(\pi, K, \bar{K}, \eta)$. Although both symmetries are broken in nature (as in our approach, when implementing physical masses), the construction of the effective field theories incorporates the breaking of these symmetries in a controlled way. In particular, it provides a systematic expansion in powers of $1/m_H$ (inverse heavy-meson mass) and powers of p, m_l (typical momentum and mass of the light meson). Following these ideas, we use two effective Lagrangians for the interaction of a heavy meson with light mesons and with baryons, respectively.

In the scattering with light mesons, the scalar (D, B) and vector (D^*, B^*) mesons are much heavier than the pseudoscalar meson octet $(\pi, K, \bar{K}, \eta)$. The latter have, in addition, masses smaller than the chiral scale $\Lambda_\chi \simeq 4\pi f_\pi$, where f_π is the pion decay constant. In this case one can exploit standard chiral perturbation theory for the dynamics of the (pseudo)Goldstone bosons, and add the heavy-quark mass expansion up to the desired order to account for the interactions with heavy mesons. In our case the effective Lagrangian is kept to next-to-leading order in the chiral expansion, but to leading order in the heavy-quark expansion [63,65]. From this effective Lagrangian one can compute the tree-level amplitude (or potential), which describes the scattering of a heavy meson off a light meson as worked out in Refs. [68,69]. At leading order in the heavy-quark expansion one gets a common result for all heavy mesons due to the exact heavy-flavor symmetry and heavy-quark spin symmetry (HQSS). The potential reads explicitly

$$V_{ij}^{\rm meson} = \frac{C_{0,ij}}{4f_\pi^2}(s-u) + \frac{2C_{1,ij}h_1}{3f_\pi^2} + \frac{2C_{2,ij}}{f_\pi^2}h_3(p_2\cdot p_4) + \frac{2C_{3,ij}}{f_\pi^2}h_5[(p_1\cdot p_2)(p_3\cdot p_4)+(p_1\cdot p_4)(p_2\cdot p_3)], \quad (16)$$

where $C_{n,ij}$ are numerical coefficients (fixed by chiral symmetry) which depend on the incoming i and outgoing j channels—and also on the quantum numbers $IJSC/B$ (isospin, total angular momentum, strangeness and charm/bottom). In Eq. (16) f_π is the pion decay constant in the chiral limit, and h_i are the low-energy constants at NLO in the chiral expansion (see Refs. [68,69] for details). Finally, s, u denote the Mandelstam variables and p_a the four-momentum of the a particle in the scattering $(1,2 \to 3,4)$.

For the heavy meson–baryon interaction we use an effective Lagrangian based on a low-energy realization of a t-channel vector meson exchange between mesons and baryons. In

the low-energy limit the interaction provides a generalized Weinberg-Tomozawa contact interaction as worked out in Refs. [62,64,66,67]. The effective Lagrangian obeys SU(6) spin-flavor symmetry in the light sector, plus HQSS in the heavy sector (which is preserved either the heavy quark is contained in the meson or in the baryon). The tree-level amplitude reads

$$V_{ij}^{\text{baryon}} = \frac{D_{ij}}{4 f_i f_j}(2\sqrt{s} - M_i - M_j) \times \sqrt{\frac{M_i + E_i}{2M_i}}\sqrt{\frac{M_j + E_j}{2M_j}}, \quad (17)$$

where D_{ij} are numerical coefficients which depend on the initial and final channels (i,j), as well as all the quantum numbers $IJSC/B$. In Eq. (17) f_i is the meson decay constant in the i channel, and M_i, E_i are the baryon mass and energy in the c.m. frame. From the form of this potential it is evident that HQSS is again maintained. We note again that in both V^{meson} and V^{baryon}, HQSS is eventually broken when using physical values for the heavy masses.

The tree-level amplitudes for meson-meson and meson-baryon scattering have strong limitations in the energy range in which they should be applied. It is limited for those processes in which the typical momentum transfer is low, and below any possible resonance. To increase the applicability of the scattering amplitudes and restore exact unitarity for the scattering-matrix elements, we apply a unitarization method, which consists of solving a coupled-channel Bethe-Salpeter equation for the unitarized scattering amplitude T_{ij} using the potential as a kernel,

$$T_{ij} = V_{ij} + V_{ik} G_k T_{kj}, \quad (18)$$

where G_k is the diagonal meson-meson (or meson-baryon) propagator which is regularized by dimensional regularization in the meson-meson (or meson-baryon) channel. We adopt the "on-shell" approximation to the kernel of the Bethe-Salpeter equation to reduce it into a set of algebraic equations. We refer the reader to Refs. [62,64,66–69] for technical details.

The unitarization procedure allows for the possibility of generating resonant states as poles of the scattering amplitude T_{ij}. Even when these resonances are not explicit degrees of freedom, and we do not propagate them in our PHSD simulations, they are automatically incorporated into the two-body interaction. This is an important fact, because such (intermediate) resonant states will strongly affect the scattering cross section of heavy mesons due to the presence of resonances, subthreshold states (bound states), and other effects like the opening of a new channel when a resonance is forming (Flatté effect).

To mention some particular examples, in the interaction of D, D^*, B, B^* mesons with light mesons we generate broad resonances in the $S, I, J^\pi = 0,1/2,0^+(1^+)$ channels. In the charm sector we identify them with the experimentally observed states $D_0^*(2400)$ and $D_1(2430)$ that can decay in an s-wave into $D\pi$ and $D^*\pi$, respectively. In the bottom sector we obtain analogous states $B_0(5530)$ and $B_1(5579)$, not yet identified by experiment. We also find a series of bound states in the channel $S, I, J^\pi = 1,0,0^+(1^+)$ which are identified with the $D_{s0}^*(2317)$ and the $D_{s1}(2460)$ states. Their bottom relatives $B_{s0}^*(5748)$ and $B_{s1}^*(5799)$ are again predictions.

In the meson-baryon channel, we find the experimental $\Lambda_c(2595)$ and $\Lambda_c(2625)$ charm resonances in the $S, I, J^\pi = 0,0,1/2^-(3/2^-)$ sector. In our model, the $\Lambda_c(2595)$ couples dominantly to DN and D^*N, while the $\Lambda_c(2625)$ to D^*N. Their bottom homologues are associated with the experimental $\Lambda_b(5912)$ and $\Lambda_b(5920)$ baryons seen by the LHCb Collaboration [66]. We finally mention the subthreshold states in the $S, I, J^\pi = 0,1,3/2^-$ channel, the $\Sigma_c(2550)$ and $\Sigma_b(5904)$ (that strongly couple to the $D\Delta$ and $\bar{B}\Delta$ channels, respectively). These states are the counterparts of the experimental $\Sigma^*(1670)$ in the strange sector, but have not been yet observed, so they can be taken as predictions for future measurements. Many other resonant states (especially in the meson-baryon sector) are found in the remaining scattering channels.

The resulting cross sections for the binary scattering of D, D^*, B, B^* (with any possible charged states) with $\pi, K, \bar{K}, \eta, N, \bar{N}, \Delta, \bar{\Delta}$ are implemented in the PHSD code considering both elastic and inelastic channels. Around 200 different channels are taken into account. Although the unitarization method helps to extend the validity of the tree-level amplitudes into the resonant region, one cannot trust the final cross sections for higher energies. Beyond the resonant region we adopt constant cross sections inspired by the results of the Regge analysis in the energy domain of several GeV [46], where one expects an almost flat energy dependence of the cross sections.

In Fig. 11 we present several examples of $B^{(*)-}$ meson scattering cross sections with pions and nucleons. The cross sections show a nonsmooth behavior with energy, due to the presence of several mesonic and baryonic beauty states generated dynamically, as described above. As an example, in the scattering with pions we observed the very broad resonant peak of $B_0(5530)$. The clear dip of some of the cross sections around 5830 MeV is due to the opening of the coupled channel B-η at $s^{1/2} = m_B + m_\eta$ (Flatté effect). In the B-n and B-p cross sections, we observe the presence of baryonic states around 6360 MeV in both $I = 0$ and $I = 1$ channels. The position and the width of these states as well as the coupling of these states to the main channels have been carefully analyzed in Ref. [68,69] in connection with several transport coefficients in heavy-ion collisions.

VII. RESULTS FOR HEAVY-ION REACTIONS

So far we have described the interactions of the heavy flavor produced in relativistic heavy-ion collisions with partonic and hadronic degrees of freedom. Since the matter produced in heavy-ion collisions is extremely dense, the interactions with the bulk matter suppresses heavy flavors at high p_T. On the other hand, the partonic or nuclear matter is accelerated outward (exploding), and a strong flow is generated via the interactions of the bulk particles and the repulsive scalar interaction for partons. Since the heavy flavor strongly interacts with the expanding matter, it is also accelerated outwards. Such effects of the medium on the heavy-flavor dynamics are expressed in terms of the nuclear modification factor defined

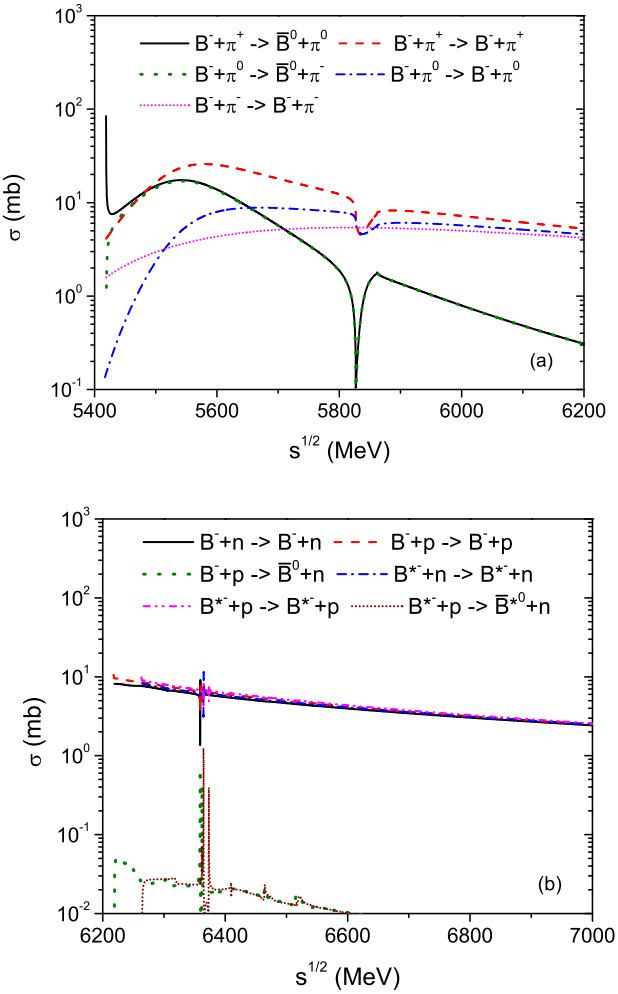

FIG. 11. Several examples of B meson scattering cross sections with pion (a) and nucleon (b).

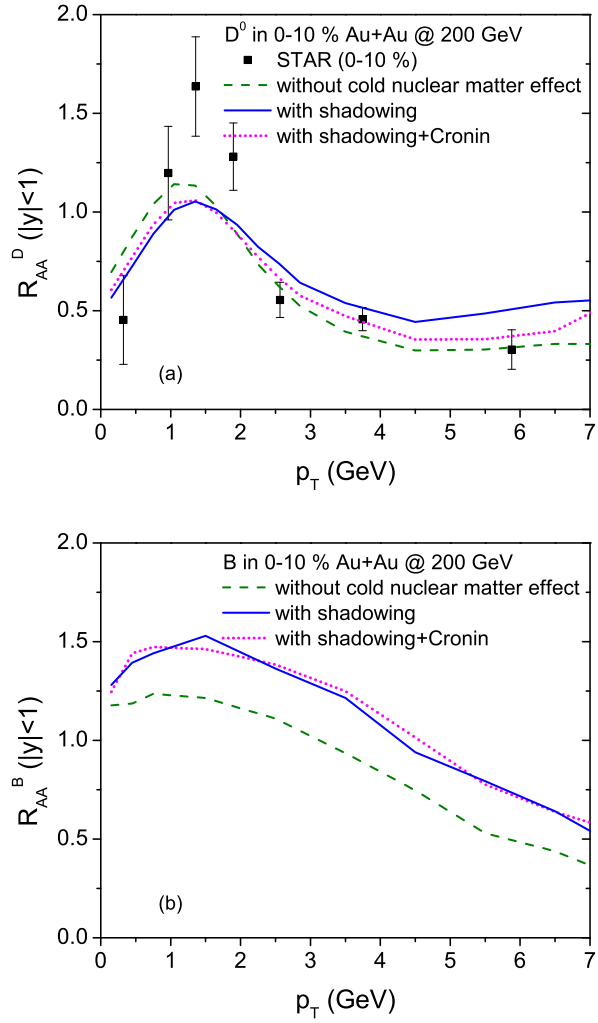

FIG. 12. $R_{\rm AA}$ of D^0 mesons (a) and of B mesons (b) with (solid) and without (dashed) shadowing effect in 0–10% central Au + Au collisions at $\sqrt{s_{\rm NN}} = 200$ GeV in comparison to the experimental data from the STAR Collaboration [33]. The dotted lines are $R_{\rm AA}$ including both shadowing and Cronin effects.

as

$$R_{\rm AA}({\rm p_T}) \equiv \frac{dN_{\rm AA}/d{\rm p_T}}{N^{\rm AA}_{\rm binary} \times dN_{\rm pp}/d{\rm p_T}}, \tag{19}$$

where $N_{\rm AA}$ and $N_{\rm pp}$ are, respectively, the number of particles produced in heavy-ion collisions and that in $p + p$ collisions, and $N^{\rm AA}_{\rm binary}$ is the number of binary nucleon-nucleon collisions in the heavy-ion collision for the centrality class considered. Note that if the heavy flavor does not interact with the medium in heavy-ion collisions, the numerator of Eq. (19) will be similar to the denominator. For the same reason, an $R_{\rm AA}$ smaller (larger) than one in a specific p_T region implies that the nuclear matter suppresses (enhances) the production of heavy flavors in that transverse momentum region.

In noncentral heavy-ion collisions the produced matter expands anisotropically due to the different pressure gradients between in plane and out of plane. If the heavy flavor interacts strongly with the nuclear matter, then it also follows this anisotropic motion to some extent. The anisotropic flow is expressed in terms of the elliptic flow v_2 which reads

$$v_2(p_T) \equiv \frac{\int d\phi \cos 2\phi (dN_{\rm AA}/dp_T d\phi)}{2\pi dN_{\rm AA}/dp_T}, \tag{20}$$

where ϕ is the azimuthal angle of a particle in momentum space.

In the following subsections, we will present our results on the production of heavy flavors and single electrons in Au + Au collisions at $\sqrt{s_{\rm NN}} = 200$ GeV, 62.4 GeV, make predictions for even lower energies, and discuss the azimuthal angular correlations between a heavy-flavor meson and its antiflavor meson.

A. Au + Au at $\sqrt{s_{\rm NN}} = 200$ GeV

The upper (a) and lower (b) panels of Fig. 12 are, respectively, the $R_{\rm AA}$ of D mesons and of B mesons in 0–10% central Au + Au collisions at $\sqrt{s_{\rm NN}} = 200$ GeV from

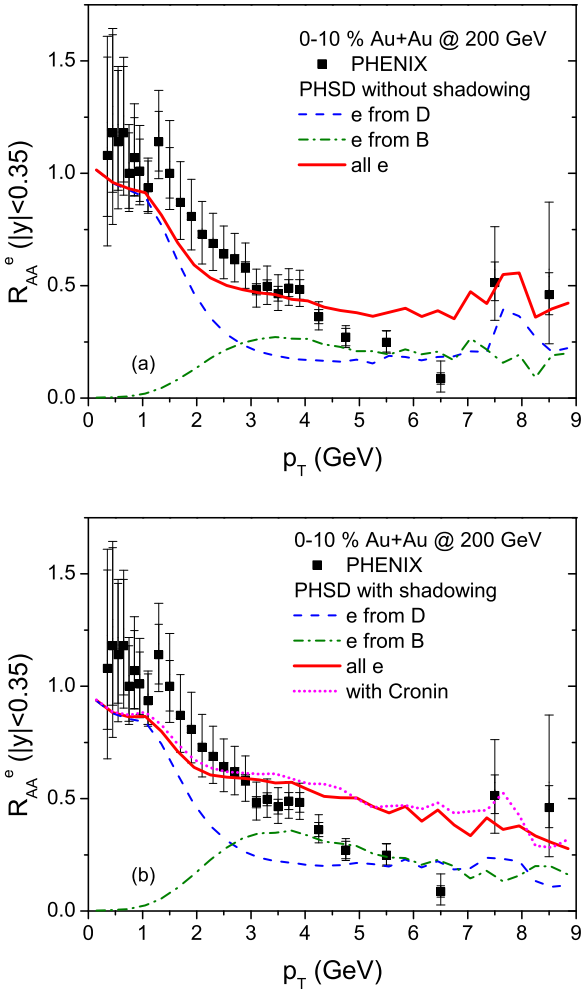

FIG. 13. R_{AA} of single electrons from the semileptonic decay of D mesons (dashed) and of B mesons (dot-dashed) and the sum of them (solid) with (b) and without (a) shadowing effect in 0–10% central Au + Au collisions at $\sqrt{s_{NN}} = 200$ GeV in comparison to the experimental data from the PHENIX Collaboration [39]. The dotted line in (b) is the R_{AA} including both shadowing and Cronin effects.

the PHSD calculations. The shadowing effect is excluded in the dashed lines and is included in the solid lines. Furthermore, in Fig. 12(a) the R_{AA} of D mesons are compared with the experimental data from the STAR Collaboration [33]. We note that the R_{AA} of D mesons without shadowing effect is slightly different from our previous results in Ref. [29], because the elastic backward scattering has been improved and the coalescence of charm quark takes place continuously as in the later work [30]. As shown in Fig. 6, the shadowing effect decreases the charm production by ∼8% and increases the bottom production by ∼20%. Apparently the R_{AA} of B mesons is much larger than that of D mesons at the same transverse momentum. However, this is attributed to the larger bottom mass than charm mass as demonstrated in Fig. 10 before.

Figure 13 shows the R_{AA} of single electrons from D-meson and B-meson semileptonic decays, which correspond to the dashed and dot-dashed lines, respectively, while the solid lines

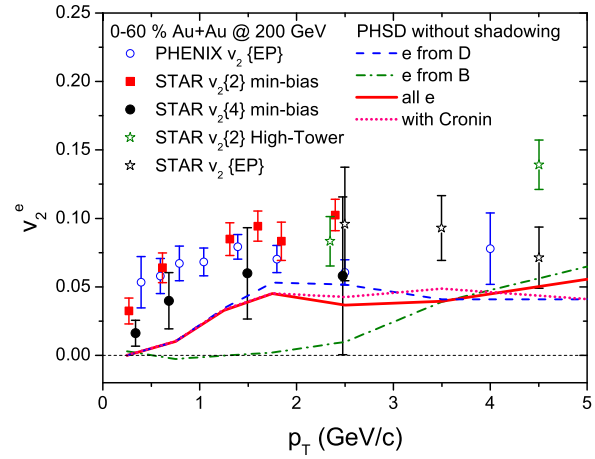

FIG. 14. The elliptic flow v_2 of single electrons from the semileptonic decay of D mesons (dashed) and of B mesons (dot-dashed) and of both of them (solid) with shadowing effect in 0–60% central Au + Au collisions at $\sqrt{s_{NN}} = 200$ GeV in comparison to the experimental data from the PHENIX and STAR Collaborations [37,38]. The dotted line is the v_2 of single electrons including both shadowing and Cronin effects.

are the sum of them in 0–10% central Au + Au collisions at $\sqrt{s_{NN}} = 200$ GeV. The upper panel (a) is the R_{AA} without shadowing effect, and the lower one (b) includes the shadowing effect, which enhances the bottom production and suppresses the charm production at low transverse momentum in line with the discussion above. We find that the single electrons from B decay have a larger contribution than that from D decay above $p_T \approx 2.7$–2.8 GeV. In $p + p$ collisions, the contribution from B decay starts to be larger than that from D decay at about $p_T \approx 4$ GeV as shown in Fig. 5. The reason for the dominance of B decay at lower transverse momentum in Au + Au collisions is that the R_{AA} of B mesons is larger than that of D mesons at high transverse momentum as shown in Fig. 12. The dotted lines in Figs. 12 and 13 are, respectively, the R_{AA} of heavy mesons and single electrons including both shadowing and Cronin effects. Although the Cronin effect enhances the R_{AA}, it is not significant.

We present in Fig. 14 the elliptic flow v_2 of single electrons with shadowing effect in 0–60% central Au + Au collisions at $\sqrt{s_{NN}} = 200$ GeV. The dashed and dot-dashed lines are, respectively, the v_2 of single electrons from D-meson and B-meson decays. Since the B meson is much more massive, the elliptic flow from B-meson decay starts to grow from much higher transverse momentum. The red lines are the elliptic flow v_2 of all single electrons. Figures 13 and 14 show that PHSD can approximately reproduce the experimental data on the R_{AA} but slightly underestimates the v_2 of single electrons from D mesons and B mesons at $\sqrt{s_{NN}} = 200$ GeV. They also show that the shadowing effect is not so critical in reproducing experimental data, which is different from the LHC energies [30].

B. Au + Au at $\sqrt{s_{NN}} = 62.4$ GeV

The beam energy scan (BES) program at RHIC has been carried out by colliding Au nuclei at various energies down

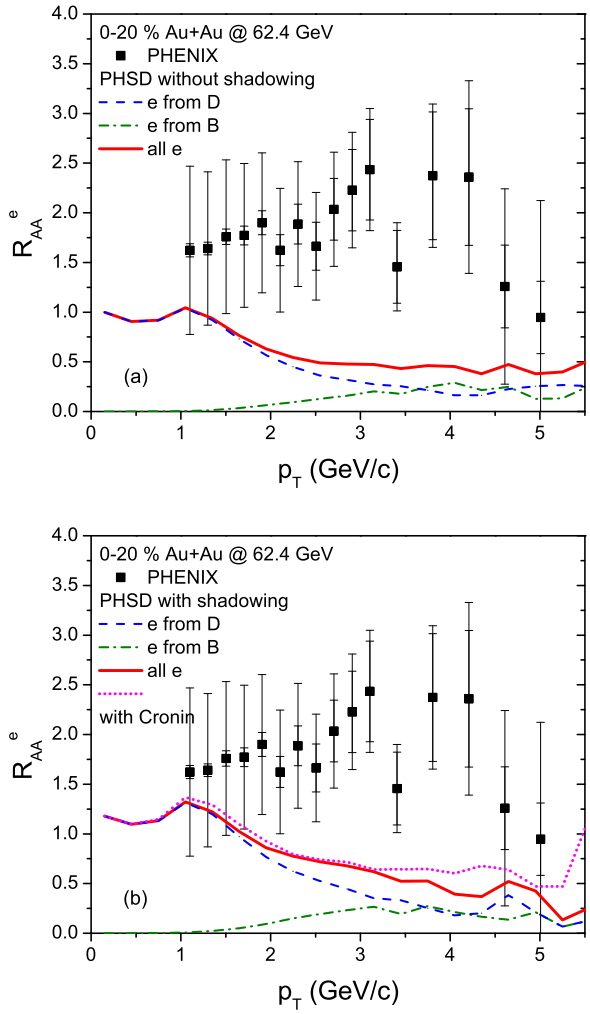

FIG. 15. R_{AA} of single electrons from the semileptonic decay of D mesons (dashed) and of B mesons (dot-dashed) and the sum of them (solid) with (b) and without (a) shadowing effect in 0–20% central Au + Au collisions at $\sqrt{s_{NN}} = 62.4$ GeV in comparison to the experimental data from the PHENIX Collaboration [39]. The dotted line in (b) is the R_{AA} including both shadowing and Cronin effects.

to $\sqrt{s_{NN}} = 7.7$ GeV. The aim of the program is to find information on the phase boundary and hopefully the critical point in the QCD phase diagram as pointed out in Refs. [4,5]. It is expected that if the trajectories of the produced nuclear matter in the QCD phase diagram pass close to the critical point, some drastic changes of observables could be measured in experiments. Since the PHENIX and STAR Collaborations recently measured the single electrons from heavy-flavor decay at $\sqrt{s_{NN}} = 62.4$ GeV [38,39], which is much lower than the maximum energy at RHIC, we first address this system in the present subsection.

Figures 15 and 16 show, respectively, the R_{AA} and elliptic flow v_2 of single electrons from the semileptonic decay of heavy flavors in 0–20% and 0–60% central Au + Au collisions at $\sqrt{s_{NN}} = 62.4$ GeV. The upper panel (a) is the results without shadowing effect and the lower one (b) with the shadowing effect. As at $\sqrt{s_{NN}} = 200$ GeV, the contribution from D-meson decay is important at low transverse momentum and

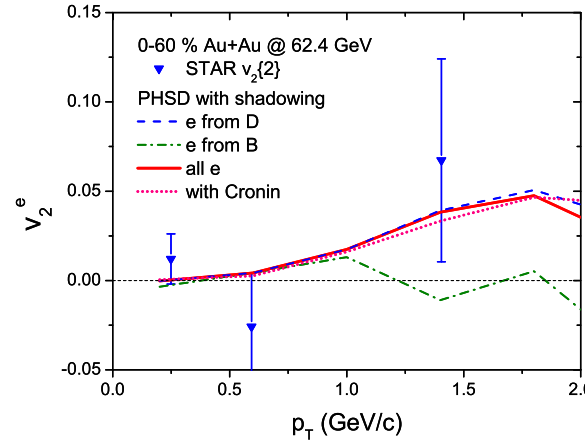

FIG. 16. The elliptic flow v_2 of single electrons from the semileptonic decay of D mesons (dashed) and of B mesons (dot-dashed) and of both of them (solid) with shadowing effect in 0–60% central Au + Au collisions at $\sqrt{s_{NN}} = 62.4$ GeV in comparison to the experimental data from the STAR Collaboration [38]. The dotted line is the v_2 of single electrons including both shadowing and Cronin effects.

superseded by the contribution from B decay above 3 GeV. The contribution from B decay becomes dominant at higher transverse momentum than at $\sqrt{s_{NN}} = 200$ GeV, because the ratio of the scattering cross section for bottom production to that for charm production is much lower at $\sqrt{s_{NN}} = 62.4$ GeV. The latter ratio is 0.75% at $\sqrt{s_{NN}} = 200$ GeV and 0.145% at $\sqrt{s_{NN}} = 62.4$ GeV according to the FONLL calculations [32].

Our PHSD results in Fig. 15 underestimate R_{AA} besides touching the lower error bars of the experimental data at low and high p_T. Although the shadowing and Cronin effects enhance R_{AA} at low p_T, there is still a large discrepancy between the experimental data and our results in the range of p_T between 2.5 and 4 GeV, which clearly lacks an explanation. We mention that a similar pattern of results has been shown in Ref. [16].

In spite of the difficulty in reproducing R_{AA}, the elliptic flow v_2 of single electrons at $\sqrt{s_{NN}} = 62.4$ GeV is well described by the PHSD approach irrespective of whether or not the shadowing effect is included, as shown in Fig. 16. The v_2 of single electrons from B-meson decay is small at low transverse momentum for the same reason as at $\sqrt{s_{NN}} = 200$ GeV.

C. Predictions at lower energies

Presently there are only few available experimental data on open heavy flavors below $\sqrt{s_{NN}} = 62.4$ GeV from the BES program. Accordingly, we will make a prediction on the production of D mesons and of single electrons at $\sqrt{s_{NN}} = 19.2$ GeV and compare again with the results at $\sqrt{s_{NN}} = 200$ and 62.4 GeV in order to obtain some excitation function.

The upper (a) and lower (b) panels of Fig. 17, respectively, show the R_{AA} of D mesons and that of single electrons in 0–10% central Au + Au collisions at $\sqrt{s_{NN}} = 200$, 62.4, and 19.2 GeV. For simplicity, the shadowing effect is not taken into account in these PHSD calculations. Comparing the R_{AA} of D mesons at $\sqrt{s_{NN}} = 200$ and 62.4 GeV, the peak of the R_{AA}

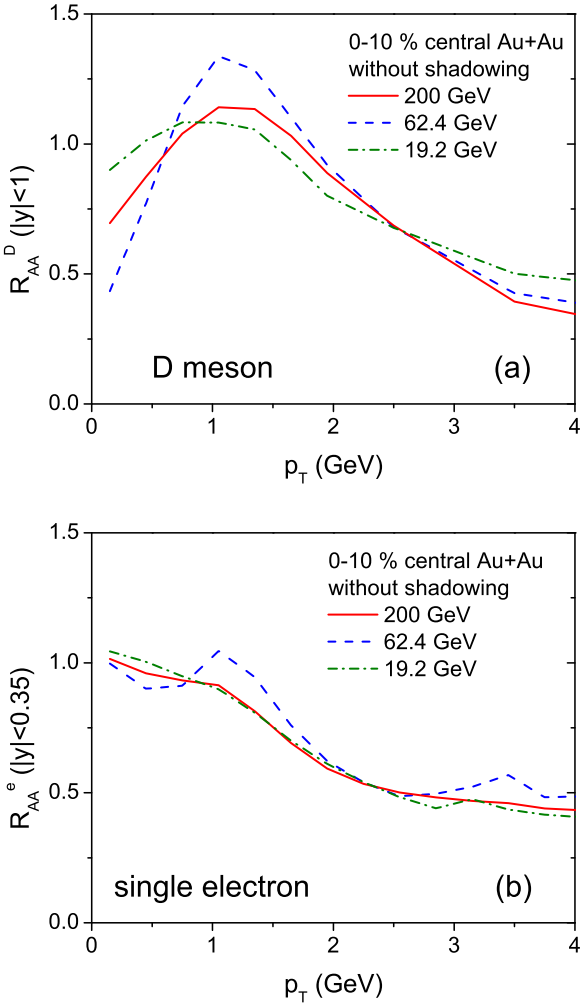

FIG. 17. R_{AA} of D mesons (b) and of single electrons (a) without shadowing effect in 0–10% central Au + Au collisions at $\sqrt{s_{NN}} =$ 200 GeV (solid), 62.4 GeV (dashed), and 19.2 GeV (dot-dashed) from the PHSD approach.

at 200 GeV is slightly shifted to higher p_T than at 62.4 GeV. On the other hand, the R_{AA} of D mesons is more highly peaked at $\sqrt{s_{NN}} = 62.4$ GeV and the same higher peak is seen in the R_{AA} of single electrons in the lower panel (b) of Fig. 17. We note that the higher peak of the R_{AA} at $\sqrt{s_{NN}} = 62.4$ GeV is attributed to the initial spectrum of heavy quarks shown in Figs. 1 and 2. For example, if the same charm quarks produced in $p + p$ collisions at $\sqrt{s_{NN}} = 200$ GeV are used as the initial charm quarks in Au + Au collisions at $\sqrt{s_{NN}} = 200$ and 62.4 GeV, the enhancement of the R_{AA} peak at $\sqrt{s_{NN}} = 62.4$ GeV is not observed any more. The peak is rather shifted to slightly lower transverse momentum, compared to the R_{AA} at $\sqrt{s_{NN}} =$ 200 GeV. As for the R_{AA} at $\sqrt{s_{NN}} = 19.2$ GeV, it is peaked at lower p_T for D mesons as well as for single electrons because of the smaller transverse flow. Comparing two panels of Fig. 17 shows that the clear structure of R_{AA} of D mesons at low transverse momentum smears in the R_{AA} of single electrons.

If a heavy quark is produced in the corona region, it will escape from the interaction zone produced in heavy-ion collisions. We show in Fig. 18 (by the solid line) the

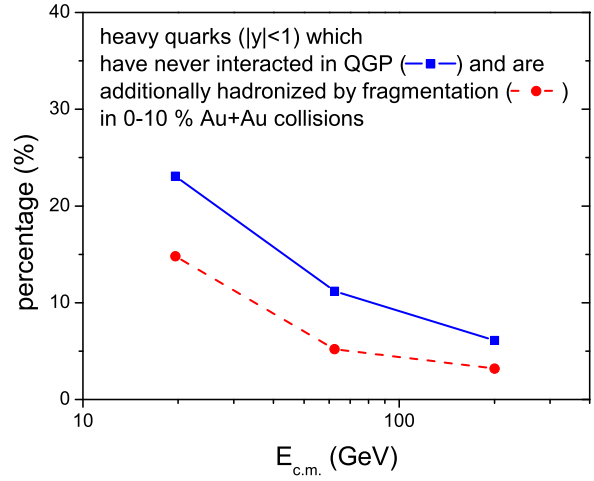

FIG. 18. The percentages of heavy quarks at midrapidity ($|y| <$ 1) with no interactions in the QGP (solid) and additional hadronization by fragmentation (dashed) in 0–10% central Au + Au collisions as a function of collision energy.

percentages of heavy quarks at midrapidity ($|y| < 1$) with no interactions with other partons in 0–10% central Au + Au collisions as a function of collision energy. The percentages are 23.1, 11.2, and 6.1% at $\sqrt{s_{NN}} = 19.2$, 62.4, and 200 GeV, respectively, demonstrating the decreasing role of the corona with bombarding energy that goes along with an increasing partonic fraction of the "fireball." Since parton coalescence is some kind of medium effect—not existing in $p + p$ collisions—we should interpret it as being generated by interactions with the medium. The dashed line in the figure is the percentage of heavy flavors at midrapidity ($|y| < 1$) with no interactions in the QGP and which are additionally hadronized by fragmentation. The percentages drop down from 14.8, 5.2, and 3.2%, respectively. This again demonstrates the effects from a larger (and longer) QGP phase of the interaction zone with increasing bombarding energy.

Figure 19 shows the transverse momentum gain or loss of charm quarks per unit time at midrapidity ($|y| < 1$) and energy density of central regions as functions of time in 0–10% central Au + Au collisions at $\sqrt{s_{NN}} = 19.2$, 62.4, and 200 GeV. We can see that a considerable energy and transverse momentum loss happens in the initial stage of heavy-ion collisions, because the energy density is extremely large as shown in panel (d). For $\sqrt{s_{NN}} = 19.2$ GeV, however, the momentum loss is delayed, since it takes some time for two Au nuclei to pass through each other and produce charm quarks. On the other hand, charm quarks, which have initially low transverse momentum, gain momentum due to the thermal motion of nuclear matter, which is larger at higher collision energies.

D. Azimuthal angular correlations

Finally we analyze the azimuthal angle between the transverse momentum of a heavy-flavor meson and that of an antiheavy-flavor meson for each heavy-flavor pair before and after the interactions with the medium in relativistic heavy-ion collisions. It is suggested that the analysis of the azimuthal angular correlation might provide information on the energy

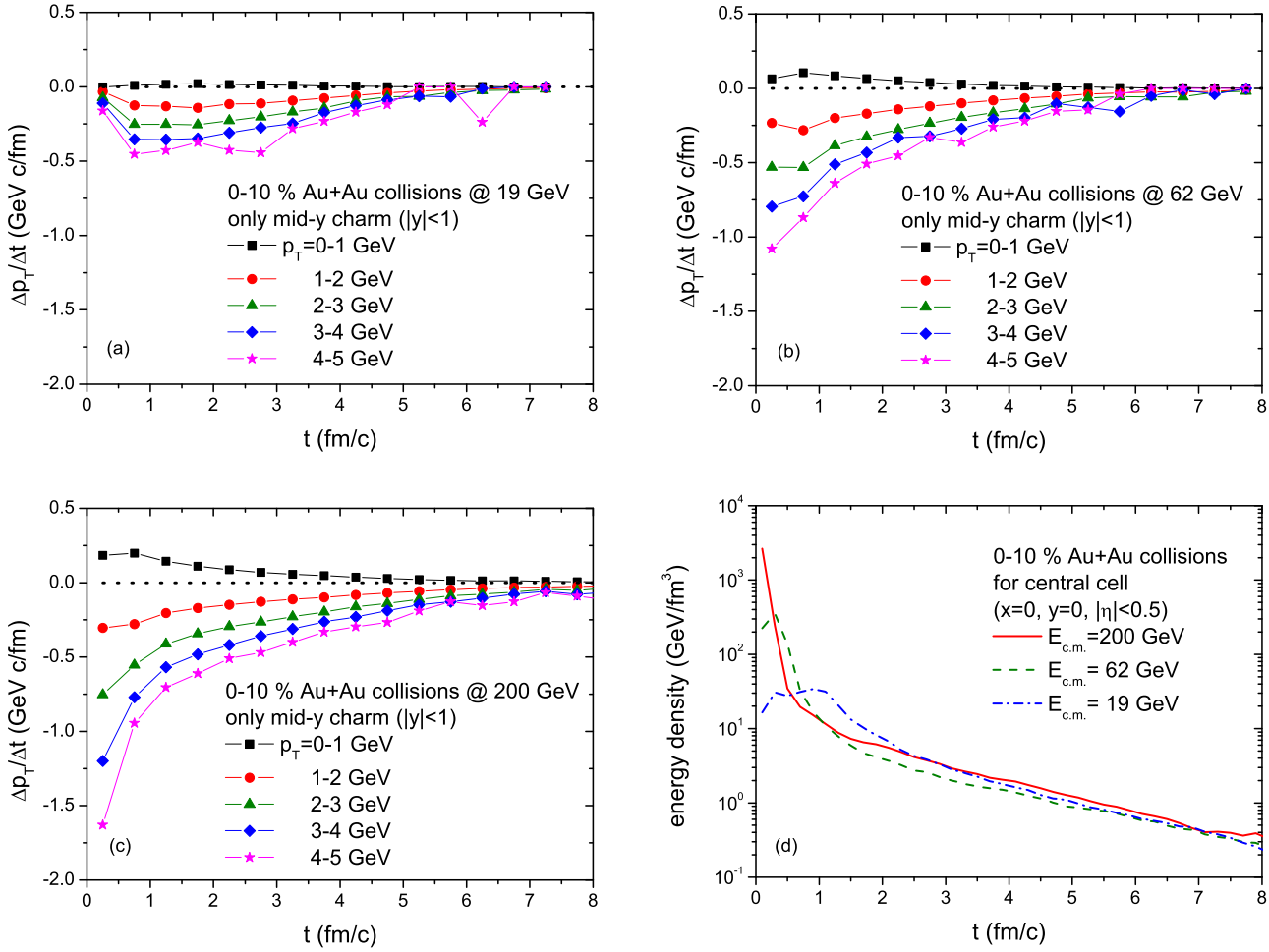

FIG. 19. Transverse momentum gain or loss of charm quarks per unit time at midrapidity ($|y| < 1$) in 0–10% central Au + Au collisions at $\sqrt{s_{\rm NN}} = 19.2$ GeV (a), 62.4 GeV (b), and 200 GeV (c) and the energy density of the central cell as functions of time at each collision energy (d) from the PHSD approach.

loss mechanism of heavy quarks in the QGP [71] because stronger interactions should result in less pronounced angular correlations. Since in the PHSD we can follow up the fate of an initial heavy quark-antiquark pair throughout the partonic scatterings, the hadronization and final hadronic rescatterings, the microscopic calculations allow us to shed some light on the correlation between the in-medium interactions and the final angular correlations.

Figure 20 shows the azimuthal angular distributions of charm and bottom pairs, respectively, in the upper left (a) and lower left (d) panels at midrapidity ($|y| < 1$) in 0–10% central Au + Au collisions at $\sqrt{s_{\rm NN}} = 200$ GeV. The dashed lines are the correlations before the interactions with the medium in heavy-ion collisions and the solid lines are those after freeze-out of the final heavy mesons. The initial azimuthal correlation of charm pairs—produced by the PYTHIA event generator—is far from back-to-back due to the associated production of further quark-antiquark pairs. The distribution in the azimuthal angles spreads widely from 0 to π although slightly more populated close to $\phi = \pi$ (back-to-back). We recall that if a heavy-quark pair is produced to the leading order in pQCD, the heavy quark and heavy antiquark are back-to-back (or close to it) in the transverse plane, assuming the transverse momentum of partons—producing the pair—to be small. However, the PYTHIA event generator also takes into account the gluon splitting ($g \to Q\bar{Q}$) which is populated near $\phi = \pi$ and the heavy quark excitation ($gQ \to gQ$) where a heavy quark or heavy antiquark is produced from the parton distribution of the colliding nucleon [31]. As a result, the initial charm pairs from PYTHIA have a mild dependence on ϕ at the energy $\sqrt{s_{\rm NN}} = 200$ GeV. In the case of bottom quarks, however, the initial pairs from PYTHIA are manifestly peaked near $\phi = \pi$, as shown in the lower left panel (d) of Fig. 20, because the contribution from gluon splitting and heavy quark excitation is small compared to charm at $\sqrt{s_{\rm NN}} = 200$ GeV.

After the initial production the heavy-flavor partons strongly interact with the medium in relativistic heavy-ion collisions. Figure 18 shows that more than 97% of the heavy quarks interact by scattering or coalescence with other partons at $\sqrt{s_{\rm NN}} = 200$ GeV. Accordingly, the azimuthal angular correlation between the initial heavy quark and heavy antiquark is washed out to a large extent.

In order to investigate the effect of the in-medium interactions on the initial heavy-quark–antiquark correlations we

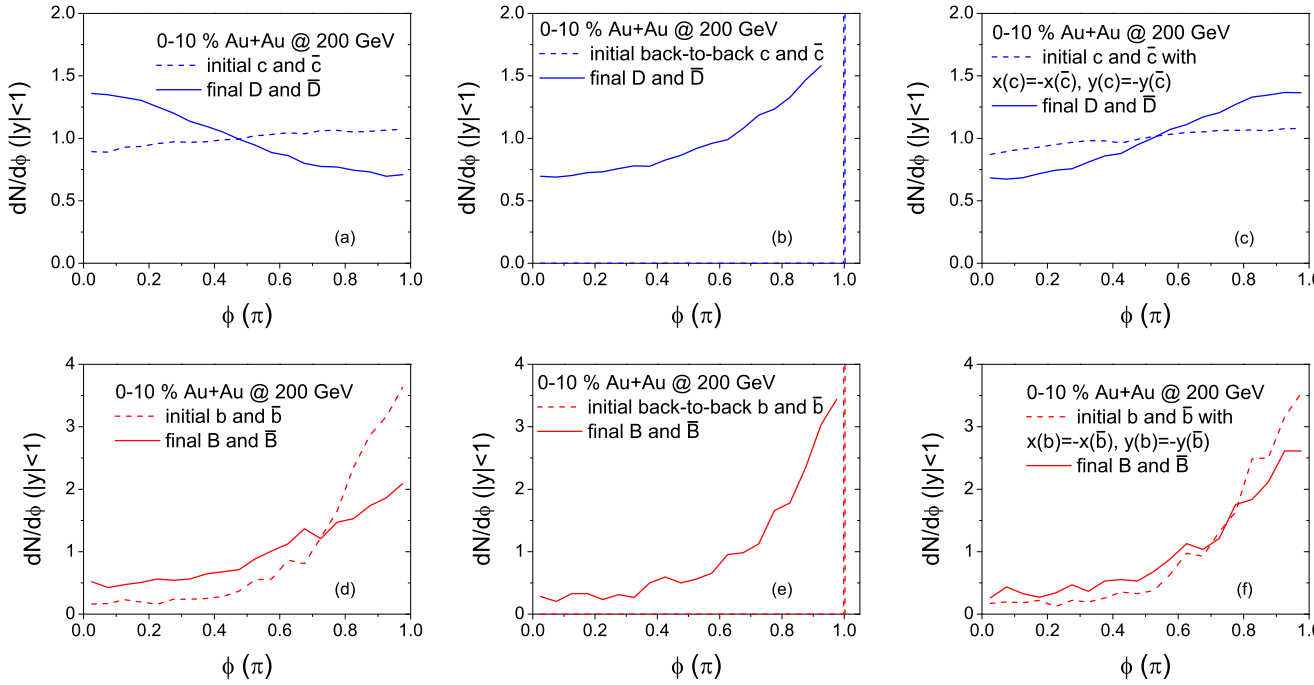

FIG. 20. The azimuthal angular correlation of initial c and $\bar{c}$ quarks (upper dashed) and final D and $\bar{D}$ mesons (upper solid) and that of initial b and $\bar{b}$ quarks (lower dashed) and final B and $\bar{B}$ mesons (lower solid) at midrapidity ($|y| < 1$) in 0–10% central Au + Au collisions at $\sqrt{s_{\rm NN}} = 200$ GeV. Panels (a) and (d) are from normal initial conditions, (b) and (e) from initial back-to-back heavy quark pairs, and (c) and (f) with the initial transverse position of the heavy antiquark being opposite to that of the heavy quark in order to investigate the flow effect on the angular correlation.

have performed a model study where the initial heavy-quark pairs are always produced back-to-back ($\phi = \pi$). Although the initial correlations are all located at $\phi = \pi$, the correlations for charm pairs disappear after the interactions with the medium in heavy-ion collisions as seen from the upper middle panel (b) of Fig. 20. However, the lower middle panels (e) of Fig. 20 show that the initial angular correlation of bottom pairs survives to some extent, because the bottom quark is too heavy to change the direction of motion in elastic scattering.

In the upper left panel of Fig. 20(a), we can see that the azimuthal angular correlation is remarkably enhanced near $\phi = 0$, which implies that the D and $\bar{D}$ mesons, which are produced as one pair in the initial stage, move in a similar transverse directions at freeze-out. A possible reason for this behavior is the transverse flow: A pair of charm and anticharm quarks are produced at the same point through a nucleon-nucleon binary collision. In the case that the scattering cross sections of charm and anticharm quarks are large such that they are stuck in the medium and not separated far from each other, they will be affected by similar transverse flows, because the flow will depend on the position of the particles. Only in case the charm and anticharm quarks are separated far enough to be located at completely different transverse positions until the transverse flow is generated in heavy-ion collisions, the collective flows of charm and anticharm quarks, respectively, will be independent.

In order to investigate in particular the flow effect on the angular correlation, we reflect the transverse position of the initial heavy antiquark with respect to the origin in right panels of Fig. 20. Since it is a reflection of the transverse position, the initial azimuthal angular correlation in momentum space does not change. However, we find that the distribution of azimuthal angles between the final D and $\bar{D}$ mesons from the same pair is completely opposite to that without the reflection, which are shown, respectively, in the upper panels (a) and (c) of Fig. 20. If the charm and anticharm quarks from one pair can move a considerable distance and be separated far enough from each other before the transverse flow is developed, the results with and without the reflection should be similar. But the results in Fig. 20 indicate that the interaction of charm and anticharm quarks with the medium is strong and they get stuck in the nuclear matter and flow together. Accordingly, the results in the panel (a) of Fig. 20—indicating that the charm and anticharm quarks from one pair exhibit similar flows depending on position—are naturally explained due to common collective flow.

VIII. SUMMARY

We have studied single electron production through the semileptonic decay of heavy mesons in relativistic heavy-ion collisions at $\sqrt{s_{\rm NN}} = 200$, 62.4, and 19.2 GeV within the PHSD transport approach. The ratio of the initial scattering cross section for bottom production to that for charm production at these collision energies is less than 1%. However, since the p_T spectrum of bottom quarks is harder than that of charm quarks and the single electrons from B-meson decay is much more energetic than that from D-meson decay, it is essential to take B-meson production into account in order to study the single electron production, especially at high p_T.

The parton-hadron-string dynamics (PHSD) approach has been employed since it successfully describes D-meson production in relativistic heavy-ion collisions at RHIC and LHC energies [29,30]. In this work, we have extended the PHSD to B-meson production and compared single electron production from heavy-meson decays with the experimental data from the PHENIX Collaboration, because there are no experimental data exclusively for B mesons at the RHIC energies.

In analogy to the charm quark pairs, the bottom pairs are produced by using the PYTHIA event generator which is tuned to reproduce the p_T spectrum and rapidity distribution of bottom quark pairs from the FONLL calculations. The (anti)shadowing effect, which is the modification of the nucleon parton distributions in a nucleus, is implemented by means of the EPS09 package. We have found that the (anti)shadowing effect is not so strong at RHIC energies as compared to LHC energies [30].

The charm and bottom partons—produced by the initial hard nucleon-nucleon scattering—interact with the massive quarks and gluons in the QGP by using the scattering cross sections calculated in the dynamical quasiparticle model (DQPM) which reproduces heavy-quark diffusion coefficients from lattice QCD calculations at temperatures above the deconfinement transition. When approaching the critical energy density for the phase transition from above, the charm and bottom (anti)quarks are hadronized into D and B mesons through the coalescence with light (anti)quarks. Those heavy quarks, which fail in coalescence until the local energy density is below $0.4\,\mathrm{GeV/fm^3}$, hadronize by fragmentation as in $p+p$ collisions. The hadronized D and B mesons then interact with light hadrons in the hadronic phase with cross sections that have been calculated in an effective Lagrangian approach with heavy-quark spin symmetry. Finally, after freeze-out of the D and B mesons they produce single electrons through semileptonic decays with the branching ratios given by the Particle Data Group (PDG).

We have found that the coalescence probability for bottom quarks is still large at high p_T compared to charm quarks, and the R_{AA} of B mesons is larger than that of D mesons at the same (high) p_T. However, this can dominantly be attributed to the much larger mass of the bottom quark. If the coalescence probability and the R_{AA} are expressed as a function of the transverse velocity of the heavy quark, both charm and bottom coalescence become similar since both are comoving with the neighboring light antiquarks.

Furthermore, we found that the PHSD approach can roughly reproduce the experimental data on single electron production in $d+\mathrm{Au}$ and $\mathrm{Au}+\mathrm{Au}$ collisions at $\sqrt{s_{\mathrm{NN}}}=200$ GeV and the elliptic flow of electrons at $\sqrt{s_{\mathrm{NN}}}=62.4$ GeV from the PHENIX Collaboration. However, the R_{AA} at $\sqrt{s_{\mathrm{NN}}}=62.4$ GeV is clearly underestimated which presently remains as an open puzzle. We have additionally made predictions for D-meson and single electron production in $\mathrm{Au}+\mathrm{Au}$ collisions at $\sqrt{s_{\mathrm{NN}}}=19.2$ GeV which can be controlled by experiment in the future.

Finally, we have studied the medium modifications of the azimuthal angular correlation of heavy-flavor pairs in central $\mathrm{Au}+\mathrm{Au}$ collisions at $\sqrt{s_{\mathrm{NN}}}=200$ GeV. Here it has been found that the initial azimuthal angular correlation of charm pairs is completely washed out during the evolution of the heavy-ion collision, even in the case where they are assumed to be initially produced back-to-back. This decoherence could be traced back to the transverse flow which drives charm pairs (close in space) into the same direction such that the azimuthal angular correlation is enhanced around $\phi=0$. By considering that the direction of the transverse flow essentially depends on position, the charm and anticharm quarks from each pair apparently are not sufficiently separated from each other before the transverse flow is developed. This decorrelation thus can be attributed to the strong interactions of charm with the medium produced in relativistic heavy-ion collisions. On the other hand, the focusing of pairs around $\phi=0$ is not observed for bottom pairs at RHIC energies due to their significantly higher mass which prevents the bottom quarks (and mesons) to change their momentum substantially in the scattering processes.

ACKNOWLEDGMENTS

The authors acknowledge inspiring discussions with J. Aichelin, S. Brodsky, P. B. Gossiaux, and P. Moreau. This work was supported by DFG under Contract No. BR 4000/3-1 and by the LOEWE center "HIC for FAIR." The computational resources were provided by the LOEWE-CSC. L.T. acknowledges support from the Ramón y Cajal research program and Grant No. FPA2013-43425-P from Ministerio de Economia y Competitividad. J.M.T.R. acknowledges the financial support from a Helmholtz Young Investigator Group VH-NG-822 from the Helmholtz Association and GSI. D.C. acknowledges support from Grant No. FIS2014-51948-C2-1-P from Ministerio de Economia y Competitividad, Spain.

[1] C. Bernard, T. Burch, C. DeTar, J. Osborn, S. Gottlieb, E. B. Gregory, D. Toussaint, U. M. Heller, and R. Sugar (MILC Collaboration), Phys. Rev. D **71**, 034504 (2005).
[2] Y. Aoki, G. Endrodi, Z. Fodor, S. D. Katz, and K. K. Szabo, Nature (London) **443**, 675 (2006).
[3] A. Bazavov, T. Bhattacharya, M. Cheng, C. DeTar, H. T. Ding, S. Gottlieb, R. Gupta, P. Hegde *et al.*, Phys. Rev. D **85**, 054503 (2012).
[4] B. Mohanty (STAR Collaboration), J. Phys. G **38**, 124023 (2011).
[5] L. Kumar (STAR Collaboration), J. Phys. G **38**, 124145 (2011).
[6] B. Abelev *et al.* (ALICE Collaboration), J. High Energy Phys. 09 (2012) 112.
[7] B. Abelev *et al.* (ALICE Collaboration), Phys. Rev. Lett. **111**, 102301 (2013).
[8] G. D. Moore and D. Teaney, Phys. Rev. C **71**, 064904 (2005).
[9] B. Zhang, L. W. Chen, and C. M. Ko, Phys. Rev. C **72**, 024906 (2005).
[10] D. Molnar, Eur. Phys. J. C **49**, 181 (2007).

[11] O. Linnyk, E. L. Bratkovskaya, and W. Cassing, Int. J. Mod. Phys. E **17**, 1367 (2008).
[12] P. B. Gossiaux, J. Aichelin, T. Gousset, and V. Guiho, J. Phys. G **37**, 094019 (2010).
[13] M. Nahrgang, J. Aichelin, P. B. Gossiaux, and K. Werner, Phys. Rev. C **90**, 024907 (2014).
[14] M. He, R. J. Fries, and R. Rapp, Phys. Rev. C **86**, 014903 (2012).
[15] M. He, R. J. Fries, and R. Rapp, Phys. Rev. Lett. **110**, 112301 (2013).
[16] M. He, R. J. Fries, and R. Rapp, Phys. Rev. C **91**, 024904 (2015).
[17] J. Uphoff, O. Fochler, Z. Xu, and C. Greiner, Phys. Rev. C **84**, 024908 (2011).
[18] J. Uphoff, O. Fochler, Z. Xu, and C. Greiner, Phys. Lett. B **717**, 430 (2012).
[19] S. Cao and S. A. Bass, Phys. Rev. C **84**, 064902 (2011).
[20] S. Cao, Nucl. Part. Phys. Proc. **276-278**, 60 (2016).
[21] S. K. Das, F. Scardina, S. Plumari, and V. Greco, Phys. Lett. B **747**, 260 (2015).
[22] M. Nahrgang, J. Aichelin, P. B. Gossiaux, and K. Werner, Phys. Rev. C **93**, 044909 (2016).
[23] A. Andronic *et al.*, Eur. Phys. J. C **76**, 107 (2016).
[24] F. Prino and R. Rapp, J. Phys. G **43**, 093002 (2016).
[25] W. Cassing and E. L. Bratkovskaya, Nucl. Phys. A **831**, 215 (2009).
[26] O. Linnyk, E. Bratkovskaya, and W. Cassing, Prog. Part. Nucl. Phys. **87**, 50 (2016).
[27] E. L. Bratkovskaya, W. Cassing, V. P. Konchakovski, and O. Linnyk, Nucl. Phys. A **856**, 162 (2011).
[28] V. P. Konchakovski, W. Cassing, and V. D. Toneev, J. Phys. G **42**, 055106 (2015); V. P. Konchakovski, E. L. Bratkovskaya, W. Cassing, V. D. Toneev, and V. Voronyuk, Phys. Rev. C **85**, 011902 (2012); V. P. Konchakovski, E. L. Bratkovskaya, W. Cassing, V. D. Toneev, S. A. Voloshin, and V. Voronyuk, *ibid.* **85**, 044922 (2012); V. P. Konchakovski, W. Cassing, Y. B. Ivanov, and V. D. Toneev, *ibid.* **90**, 014903 (2014).
[29] T. Song, H. Berrehrah, D. Cabrera, J. M. Torres-Rincon, L. Tolos, W. Cassing, and E. Bratkovskaya, Phys. Rev. C **92**, 014910 (2015).
[30] T. Song, H. Berrehrah, D. Cabrera, W. Cassing, and E. Bratkovskaya, Phys. Rev. C **93**, 034906 (2016).
[31] T. Sjostrand, S. Mrenna, and P. Z. Skands, J. High Energy Phys. 05 (2006) 026.
[32] M. Cacciari, S. Frixione, N. Houdeau, M. L. Mangano, P. Nason, and G. Ridolfi, J. High Energy Phys. 10 (2012) 137.
[33] L. Adamczyk *et al.* (STAR Collaboration), Phys. Rev. Lett. **113**, 142301 (2014).
[34] D. Tlusty (STAR Collaboration), Nucl. Phys. A **904-905**, 639c (2013).
[35] J. Adam *et al.* (ALICE Collaboration), J. High Energy Phys. 03 (2016) 081.
[36] B. B. Abelev *et al.* (ALICE Collaboration), Phys. Rev. C **90**, 034904 (2014).
[37] A. Adare *et al.* (PHENIX Collaboration), Phys. Rev. Lett. **98**, 172301 (2007).
[38] L. Adamczyk *et al.* (STAR Collaboration), Phys. Rev. C **95**, 034907 (2017).
[39] A. Adare *et al.* (PHENIX Collaboration), Phys. Rev. C **91**, 044907 (2015).
[40] L. Adamczyk *et al.* (STAR Collaboration), Phys. Rev. D **86**, 072013 (2012).
[41] C. Peterson, D. Schlatter, I. Schmitt, and P. M. Zerwas, Phys. Rev. D **27**, 105 (1983).
[42] J. Abdallah *et al.* (DELPHI Collaboration), Eur. Phys. J. C **71**, 1557 (2011).
[43] L. Gladilin, arXiv:hep-ex/9912064.
[44] S. Chekanov *et al.* (ZEUS Collaboration), J. High Energy Phys. 07 (2007) 074.
[45] B. Abelev *et al.* (ALICE Collaboration), J. High Energy Phys. 07 (2012) 191.
[46] K. A. Olive *et al.* (Particle Data Group Collaboration), Chin. Phys. C **38**, 090001 (2014).
[47] A. Adare *et al.* (PHENIX Collaboration), Phys. Rev. Lett. **97**, 252002 (2006).
[48] M. Basile *et al.*, Nuovo Cimento A **65**, 421 (1981).
[49] A. Bodek, N. Giokaris, W. B. Atwood, D. H. Coward, D. J. Sherden, D. L. Dubin, J. E. Elias, J. I. Friedman, H. W. Kendall, J. S. Poucher, and E. M. Riordan, Phys. Rev. Lett. **50**, 1431 (1983).
[50] K. J. Eskola, H. Paukkunen, and C. A. Salgado, J. High Energy Phys. 04 (2009) 065.
[51] X. Zhao and R. Rapp, Phys. Lett. B **664**, 253 (2008).
[52] X. N. Wang, Phys. Rev. Lett. **81**, 2655 (1998).
[53] W. M. Alberico, A. Beraudo, A. De Pace, A. Molinari, M. Monteno, M. Nardi, and F. Prino, Eur. Phys. J. C **71**, 1666 (2011).
[54] A. Adare *et al.* (PHENIX Collaboration), Phys. Rev. Lett. **109**, 242301 (2012).
[55] A. Adare *et al.* (PHENIX Collaboration), Phys. Rev. Lett. **112**, 252301 (2014).
[56] W. Cassing, Eur. Phys. J.: Spec. Top. **168**, 3 (2009); Nucl. Phys. A **795**, 70 (2007).
[57] H. Berrehrah, E. Bratkovskaya, W. Cassing, P. B. Gossiaux, J. Aichelin, and M. Bleicher, Phys. Rev. C **89**, 054901 (2014).
[58] H. Berrehrah, P. B. Gossiaux, J. Aichelin, W. Cassing, and E. Bratkovskaya, Phys. Rev. C **90**, 064906 (2014).
[59] H. Berrehrah, E. Bratkovskaya, T. Steinert, and W. Cassing, Int. J. Mod. Phys. E **25**, 1642003 (2016).
[60] H. Berrehrah, M. Nahrgang, T. Song, V. Ozvenchuck, P. B. Gossiaux, K. Werner, E. Bratkovskaya, and J. Aichelin, FIAS Interdisc. Sci. Ser. **9783319441658**, 151 (2017).
[61] T. Song and H. Berrehrah, Phys. Rev. C **94**, 034901 (2016).
[62] C. Garcia-Recio, V. K. Magas, T. Mizutani, J. Nieves, A. Ramos, L. L. Salcedo, and L. Tolos, Phys. Rev. D **79**, 054004 (2009).
[63] L. M. Abreu, D. Cabrera, F. J. Llanes-Estrada, and J. M. Torres-Rincon, Ann. Phys. **326**, 2737 (2011).
[64] O. Romanets, L. Tolos, C. Garcia-Recio, J. Nieves, L. L. Salcedo, and R. G. E. Timmermans, Phys. Rev. D **85**, 114032 (2012).
[65] L. M. Abreu, D. Cabrera, and J. M. Torres-Rincon, Phys. Rev. D **87**, 034019 (2013).
[66] C. Garcia-Recio, J. Nieves, O. Romanets, L. L. Salcedo, and L. Tolos, Phys. Rev. D **87**, 034032 (2013).
[67] C. Garcia-Recio, J. Nieves, O. Romanets, L. L. Salcedo, and L. Tolos, Phys. Rev. D **87**, 074034 (2013).
[68] L. Tolos and J. M. Torres-Rincon, Phys. Rev. D **88**, 074019 (2013).
[69] J. M. Torres-Rincon, L. Tolos, and O. Romanets, Phys. Rev. D **89**, 074042 (2014).
[70] L. Tolos, Int. J. Mod. Phys. E **22**, 1330027 (2013).
[71] S. Cao, G. Y. Qin, and S. A. Bass, Phys. Rev. C **92**, 054909 (2015).